Inelastic Scattering from Microparticles:
Fluorescence Microscopy and Spectroscopy of Oriented Molecules within a Levitated Microdroplet

by

Noel Lee Goddard
Microparticle Photophysics Lab (MP^3L)

THESIS

Submitted in Partial Fulfillment
of the Requirement for the
Degree of

Master's of Science (Chemistry)

Polytechnic University Brooklyn, NY 11201

Approved May 1998:

Copy Number _____

_____
Department Head

AN ABSTRACT

Inelastic Scattering from Microparticles:

Fluorescence Microscopy and Spectroscopy of Oriented Molecules within a Levitated Microdroplet

by

Noel Lee Goddard

Working Advisor: Stephen Arnold

Formal Advisor: Bruce Garetz

Submitted in Partial Fulfillment of the Requirements
for the Degree of Master of Science (Chemistry)

April 1998

Developments within the last decade in the field of Cavity Quantum Electrodynamics (CQED) have opened the door for exploring the role which the associated phenomena can have in microscopic chemical systems, as well as in the fusion between materials and photonics (e.g. micro-cavity lasers). Specialized electrodynamic levitator traps, originally developed by Arnold et al, to find the absolute mass associated with levitated particles, became the basis for levitating droplets (radius~5-10μm) in a gaseous environment -- ideal for the study of aerosol chemistry, homogeneous nucleation, and most recently, CQED effects in spherical dielectric optical cavities. Emission from microdroplets containing surfactant chromophores display radically enhanced decay rates indicative of preferential coupling between the chromophore's emission moment and the droplet's intrinsic whispering gallery modes. By altering the surface structure through molecular design, profound orientational effects are observed in the resulting emission spectra. Surfactant monolayers (~10^{-3}M) are used as scaffoldings to support the emission moment of embedded chromophores normal to the surface of the sphere. The measured fluorescence spectra are compared with a semiclassical emission rate enhancement model which treats the coupling between an excited state and Mie resonances as an oscillating dipole interacting with its self-scattered field. This theory, complemented by asymptotic formulas for the widths and strengths of the resonances, is developed into a computer program used to simulate spectra for droplet of a given optical size and chromophore emission moment orientation. Comparison of the theory against the experimental spectra confirms not only the chosen extreme orientations by design, but proves one can elucidate the heterogeneity of <u>any</u> microdroplet from its resonant structure, and determine the orientation of the emission moments relative to the phase boundary. This new

fundamental understanding promotes the development of novel technological applications such as the remote identification of microencapsulated aerosols and low-threshold lasing.

VITA

Noel L. Goddard was born in Orlando, Florida November 2, 1974 and later moved with her family to Maryville, Tennessee, Heart of the Great Smoky Mountains, where she completed her secondary schooling. In September of 1992, upon acceptance to The Cooper Union for the Advancement of Science and Art, she began pursuit of a degree in Chemical Engineering. Following an internship at the U.S. Department of Energy's Environmental Measurements Laboratory in the Organic Chemistry Division, she decided to change paths and pursue a degree in pure Chemistry; transferring to the Polytechnic University to complete her degree. Her undergraduate thesis research, *Laser Induced Nucleation in Supersaturated Urea Solutions*, under the guidance of Professor Bruce Garetz, resulted in the publication of a Physical Review Letter {77 3475-6 (1996)} and review in the Annual Edition of Optical and Photonic New's *Optics in 1997* {8 32-3 (1997)}. In June 1996, she began further undergraduate research under Professor Stephen Arnold in the Microparticle Photophysics Lab (MP^3L). After completing a double major Bachelor of Science in Chemistry and Humanities in January of 1997, she began her Master of Science in Chemistry studies at the Polytechnic again under the advisement of Dr. Garetz (Formal), and co-advisement of Professors Stephen Arnold (Working) and Alan Myerson. To date these studies have produced two publications {Mat.Sci. and Eng. B B48 139-46 (1997), and Opt.Lett.22 1452-4 (1997)} with a third in press (J. Chem. Phys., accepted Feb., 1998). This research was generously supported by the General Electric Faculty for the Future Fellowship Program, the National Science Foundation Grant No.s CTS-9625178 and ECS- 9634617, and Northrop Grumman.

Table of Contents

Table of Illustrations

I. Introduction and Goals

Over the last few years it has become apparent that spontaneous emission processes such as fluorescence and Raman can be severely modified by macroscopic structures.[1] The effect is especially pronounced in microparticles. The common belief that emission is a molecular property associated with the local environment appears to be incorrect. Our goal is to understand this effect for molecular systems so that we can make meaningful interpretations of both Fluorescence and Raman spectra in microdroplets. We concentrate here on fluorescence because its larger yield increases the relative ease with which spectra can be obtained.

Since processes such as fluorescence have varied applications from the emission of fireflies and lightbulbs, to light from the sun's surface, it is imperative that an understanding for the interaction of molecular excited states with macroscopic structures evolve. Recent fluorescence technologies have allowed us to harness our present knowledge and investigate the complexities of biological structure and function as well as single molecules[2] -- the very thread of our being.

The broad goal of this thesis was to understand inelastic scattering from microdroplets. This subject encompasses both fluorescence and Raman scattering. Each of these is spontaneous, although theory for neither has been put to a critical test in comparison with experiment. The absence of such a comparison in this classic problem stems from the unavailability of data on a well defined system. Homogeneously filled droplets have active molecular dipoles which are both random in position and in orientation. A further complication is that the droplet optics itself causes the incident light beam to generate an electromagnetic field in the interior which is extremely inhomogeneous and sensitive to differences in size. Consequently, attempting to make a critical test of theory with soluble systems (i.e. spatially homogeneous) is at present unrealistic. However a more reasonable approach is to locate and orient molecules by "molecular design".

Unfortunately the bulk of a liquid by definition cannot support molecular localization or orientation, however the surface provides an energy reduction for surfactant species which allows for a natural "home". The road to the goal of understanding inelastic scattering from surface active species is intermingled with the need to make measurements on such heterogeneous microdroplets. As a consequence this thesis project involves the design of new instrumentation as well as well as "molecular design".

II. Background

Absorption and emission spectroscopies have been a boon to chemical analysis. Although both phenomena have been appreciated for centuries, it has only been during this century that a fairly clear understanding for the absorption and emission from molecules in condensed matter has emerged. Luminescence had been observed and documented as early as 1100-1200 BC by the ancient Chinese.[3] However, the theoretical machinery for predicting luminescence lifetimes and spectra had to wait for an understanding of chemical composition, begun in the 17th century,[4] and quantum mechanics in our century. Although Pauling was able to grasp the nature of the chemical bond through Coulombic interactions in quantum mechanics, a complete understanding of luminescence requires not only the quantization of electronic states, but also interactions with photonic modes of the macroscopic structure in which the molecule is incorporated.

Absorption and emission spectra of a typical organic chromophore at room temperature are shown in Fig.1. The near mirror symmetry between these

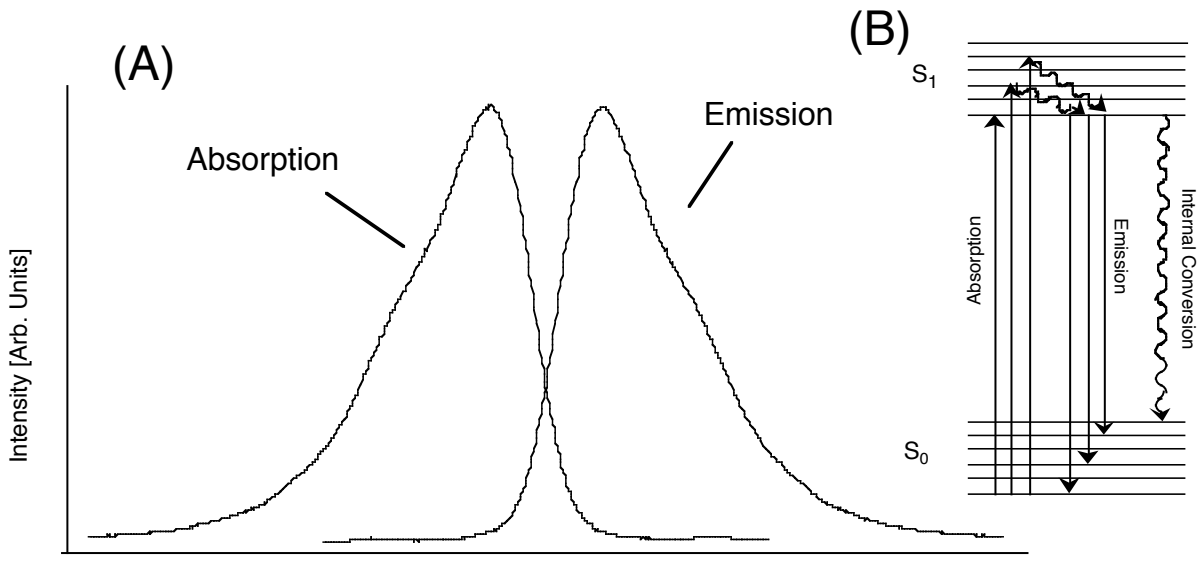

Fig.1 (A) Fluorescence absorption and emission spectra of a typical organic chromophore with (B) corresponding Jablonski Diagram representing electronic transition between the ground and excited states.

spectra is a measure of vibrational similarity in both the excited (S_1) and ground (S_0) electronic states. The spectral shape can be understood by using the Jablonski

diagram (Fig. 1B). The mechanism leading to the shape of the spectra is considered to be principally a local effect (i.e. governed by a region about the molecule less than ~ 1 nm in radius).

This local view changed in 1980 with the work of Benner et al[5] at Yale. The luminescence spectrum from a dye impregnated polystyrene hydrosol microparticle (diameter ~ 10μm) revealed the pronounced peaks shown in Fig.2.

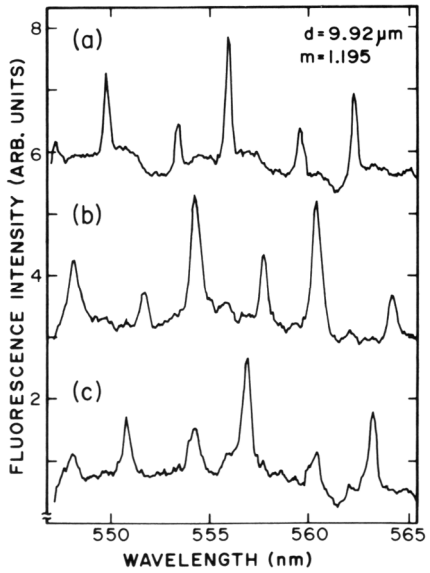

Fig.2 Fluorescence spectra for the three individual dye-impregnated polystyrene spheres in a nominally monodispersed hydrosol.[5]

The peaks were found to involve the entire structure of the microparticle. Later, Folan, et al[6] discovered enhanced energy transfer in an isolated aerosol particle, and through a series of papers,[7,8,9] proved that the effect was the consequence of a global mechanism. However throughout all of this work, never was a solid theory able to rigorously interpret or predict the resulting experimental spectrum of a particular system. This task is the subject of this thesis.

III. The Use Of Emission Spectroscopy For Determining Orientation

III.A. Development of a Semiclassical Model for Emission

Emission spectroscopy is considerably different from excitation spectroscopy. In the former, the excited molecule is the source, whereas in the latter, an external light source drives the system. We are particularly interested in emission spectroscopy because of the possibilities revealed by the peaks seen in Fig.2. Hence, it is important to understand the cause of the peaks. The most obvious notion is that the rate of emission is modified by the presence of the microsphere. In what follows I will review a model for understanding this effect.

Even before the turn of the century, scientists demonstrated that radiation results from oscillating charges (e.g. the experiments of Hertz and the wireless communication of Marconi). Similarly, on the molecular level, an electronically excited molecule which gives rise to emission may be thought of as possessing an oscillating dipole moment μ.[10] Specifically, a molecule interacting with fields at optical frequencies, for our purposes, may be thought of as a damped harmonic oscillator [i.e. a charged mass on a spring with a dashpot for damping]. The dynamics of oscillation can be modeled as

$$\ddot{\mu} + \omega_0^2 \mu + \gamma_0 \dot{\mu} = 0 \qquad (1)$$

where ω_0 is the undamped frequency of oscillation, and γ_0 is the damping rate. Although this is an adequate model to describe a simple decay, the rate obtained cannot explain the emission spectrum in Fig.2. If indeed the dipole is interacting with the particle, an additional component remains to be explored.

A possible answer lies in a related work of Hans Kuhn.[11] In 1970 Kuhn studied fixed position chromophores in Langmuir-Blodgett films. He observed that the rate of emitted radiation could be modified if a mirror was used to reflect the field back onto the emissive moment of the dipoles, as shown in Fig.3.

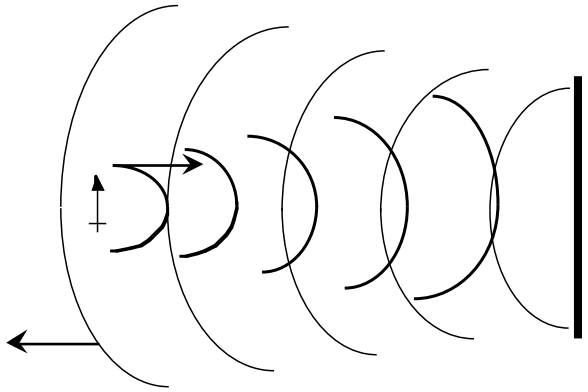

Fig.3 An oscillating dipole and its emitted field reflected by a mirror

It then becomes possible to imagine that this reflected radiation can perturb the dipole with the perturbation depending on the phase of the returning field relative to the dipole dynamics. In addition, we expect the interaction to be orientationally sensitive (i.e. a horizontally oriented dipole in the plane of Fig.3 cannot interact with the mirror as shown).

Fortunately, the simplicity of the Kuhn mechanism allows us to draw parallels in our own model. We will suppose that the amount of luminescence per unit frequency is proportional to the excited state decay rate at that frequency. The interaction between such a "semiclassical" atom and a macroscopic structure can be modeled as a damped harmonic oscillator "driven" by its own scattered field $\underline{E}_S$, and damped by the emission of radiation (i.e. radiation reaction[12]). The dynamics of the dipole positioned at $\underline{r}_d$ is described by

$$\ddot{\mu} + \gamma_0 \dot{\mu} + \omega_0^2 \mu = \frac{q^2}{m} \hat{n} \cdot \underline{E}_s \,, \tag{2}$$

where q is the magnitude of oscillating charge, m the mass, and $\hat{n}$ is a unit vector in the direction of the dipole (i.e. $\hat{n} = \underline{\mu}/\mu$). In order to see the effect which this coherent scattered field $\underline{E}_S$ has on the dynamics, it is useful to look at the characteristic equation, associated with Eqn.2, in the frequency domain. This is most readily accomplished by representing μ as $\mu_0 e^{-i\omega t}$ and $\underline{E}_S$ as $\overleftrightarrow{T}(\underline{r}_d, \underline{r}_d, \omega) \cdot \underline{\mu} = \overleftrightarrow{T}(\underline{r}_d, \underline{r}_d, \omega) \cdot \hat{n}\, \mu$, where $\overleftrightarrow{T}(\underline{r}_d, \underline{r}_d, \omega)$ is the Green's function dyadic in which both the "source" and field points are at $\underline{r}_d$. The resulting characteristic equation for ω is

$$-\omega^2 + \omega_0^2 - i\omega\gamma_0 = \frac{q^2}{m} \hat{n} \cdot \overleftrightarrow{T} \cdot \hat{n} \,. \tag{3}$$

For convenience $\hat{n}\cdot\vec{\vec{T}}\cdot\hat{n}$ will be defined alternatively as T_n . T_n is complex, since in general E_S will not be in phase with μ. Consequently, we will represent T_n as $T_{nr}+i\,T_{ni}$. Eqn.3 can be rewritten in a rather revealing way,

$$-\omega^2+\left[\omega_0^2+\frac{q^2}{m}T_{nr}\right]-i\omega\left[\gamma_0+\frac{q^2}{m\omega}T_{ni}\right]=0 \qquad (4)$$

Eqn. 4 suggests the scattered field can not only shift the frequency of the oscillator, but change its rate of decay as well. We are particularly interested in the latter. For a typical chromophore the emission frequency, ω_0, is considerably larger than the fluorescence decay rate, γ_0, or the absolute interaction strength $q^2|T_n|/m$. As a consequence, ω may be taken to be ω_0 in estimating the effective decay rate γ. From Eqn.4,

$$\gamma\approx\gamma_0+\frac{q^2}{m}\,\frac{\mathrm{Im}[\hat{n}\cdot\vec{\vec{T}}(\underline{r}_d,\underline{r}_d,\omega)\cdot\hat{n}]}{\omega_0}\ . \qquad (5)$$

This simple formula displays two important aspects of the physics. First, the rate of decay is potentially sensitive to the orientation of the dipole (i.e. perpendicular or parallel to the particle surface), as denoted by sandwiching the dyadic between the orientational unit vector $\hat{n}$. Second, the quadrature component of the scattered field controls the modification of the decay rate, through the imaginary part of the scattered field dyadic. Neither should come as a great surprise. Clearly orientation must enter. If the scattered field has no component along the dipole, it can produce no interaction. By analogy, the effect of the imaginary part is similar to the case of pushing a child on a swing. If you want the swing to lose or gain energy in the most optimal way, you push +/- 90 degrees out of phase with its displacement, and in phase or 180^o out of phase with its motion (i.e. velocity).

Eqn.5 accounts for the total rate of decay. For dielectrics with low loss and molecules having high fluorescence quantum efficiencies, each of which can be experimentally arranged, this rate will be equivalent to the radiative rate.[13] In an extended medium of refractive index, n, the radiative decay rate for an oscillating charge in Gaussian units is

$$\gamma_{rn} = \frac{2}{3}\frac{nq^2k^3}{m\omega}. \qquad (6)$$

Using this expression for γ_o in Eqn.5, we find the decay rate, relative to the radiative rate in an extended medium, to be

$$\frac{\gamma}{\gamma_{rn}} \approx 1 + \frac{3}{2k^3n}\ \mathrm{Im}[\hat{n}\cdot\overleftrightarrow{T}(\underline{r}_d, \underline{r}_d, \omega)\cdot\hat{n}]. \qquad (7)$$

Eqn.7 is a calculation of the total rate of decay. This includes both the radiative and nonradiative rate. Our interest is principally in the radiative contribution. Fortunately the nonradiative contribution due to interactions with the microdroplet will be minimal in our experiments since the dielectrics we will be dealing with are nearly transparent; the imaginary part of the refractive index is less than 10-7. 8

III.B Calculation of orientational dependence of emission spectrum

We are now in a position to evaluate Eqn.7 for an oscillating dipole positioned just below the surface of a microdroplet (Fig.4).

□

Fig.4 A dipole positioned just below the north pole of a spherical dielectric particle with an emission moment oriented at angle qm to the surface normal.

For a dipole positioned on the z-axis just within the surface of the droplet and oriented in the x-z plane, the required dyadic arrived at from an electrodynamic solution to the associated boundary value problem□ is

□

where k is the angular wavenumber in free space (i.e. 2π divided by wavelength l),

□ (9)

and

□ (10)

where □ and □ are spherical Bessel and spherical Hankel functions with mode number l. The parameter X is the optical size, X = ka =2πa/l, for a droplet of radius a, and the refractive index, n.

The coefficients TEl and TMl measure the strength of coupling to Transverse Electric (TE) and Transverse Magnetic (TM) modes respectively. TE and TM modes correspond to the distinct solution to the vector wave equation in a spherical enclosure. That there are two solutions should come as no surprise, after all the wave equation is a 2nd order differential equation. However, since electromagnetic waves are vector waves, each of the solutions has a different polarization. TE modes have no radial component in their electromagnetic field, whereas TM modes have a radial component as well as an angular component. This difference in polarization between TE and TM modes is one of the most important qualities associated with the interaction of an excited molecule with a microdroplet.

In particular, a radially oriented dipole cannot stimulate a TE mode; the dipole is perpendicular to the electric field in the mode. Such a dipole stimulates only TM modes. On the other hand, a tangentially oriented dipole (i.e. parallel to the surface) can stimulate both TE and TM modes. The importance of this will become apparent as we examine spectra.

To calculate the spectrum associated with a dipole having an arbitrary orientation □ we evaluate Eqn.7 using □ from Eqn.8.
Eqn.8.

$$\frac{\gamma(\theta,\omega)}{\gamma_{rn}} = 1 + \frac{3}{2}\,\mathrm{Re}\sum_{l=1}^{\infty}(2l+1)$$
$$\left\{ TM_l \left[l(l+1)\left(\frac{j_l(nX)}{(nX)}\right)^2 \mathrm{Cos}^2(\theta) + \frac{1}{2}\left(\frac{\left[(nX)j_l(nX)\right]'}{(nX)}\right)^2 \mathrm{Sin}^2(\theta) \right] + \frac{1}{2} TE_l\, j_l{}^2(nX)\, \mathrm{Sin}^2(\theta) \right\} \quad (11)$$

This is an good time to examine the predictions of theory (Eqn.11) for dipoles having various orientations. We explore two distinct cases. In the first we suppose that the emission moment is radial within a particle 5μm in radius and having a refractive index n=1.4. The result of the calculations is shown in Fig.5. The only peaks appearing are associated with the resonant excitation of transverse magnetic modes (TM). Although a considerable enhancement is predicted at the narrowest

resonances, off-resonance the rate of decay drops below the radiative rate in an extended medium of the same refractive index, by nearly a factor of three.

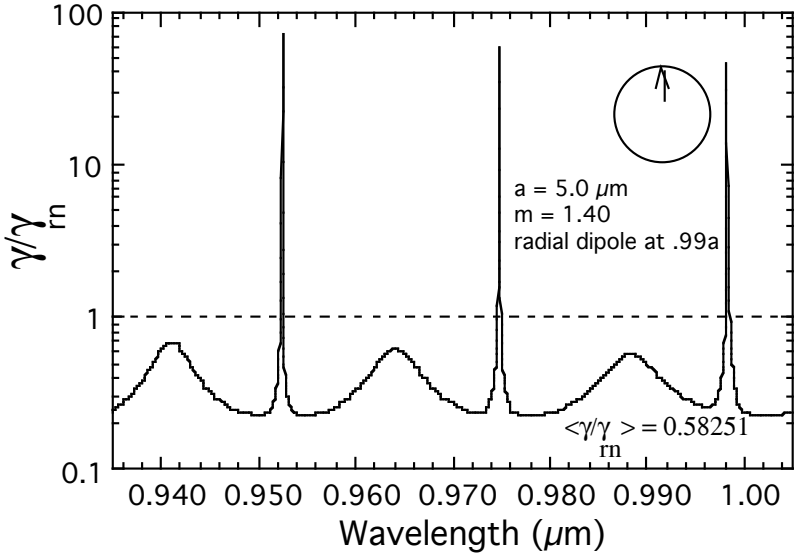

Fig.5 Calculation of the relative rate of decay for a molecule just inside the surface of a particle 5 μm in radius with its transition moment oriented radially.

The peaks in Fig. 5 may be associated with waves which circumnavigate the interior and return in phase. Consequently these peaks shift in the spectrum depending on size. If the particle increases in size the peaks will shift toward longer wavelength in proportion to the size change. Considering the narrow linewidth of the peaks (< 1 part in 10^5), a radius change <0.5 Å should be discernible for a particle ~5μm in radius.

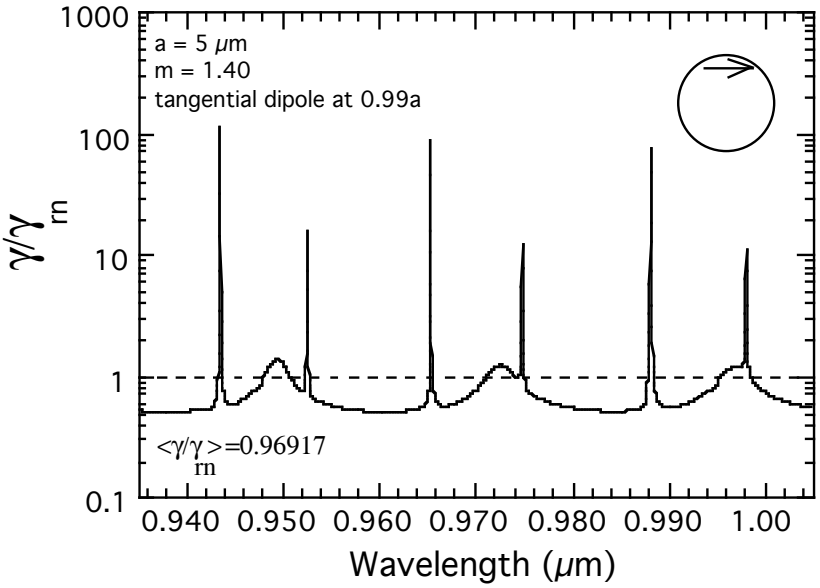

Fig.6 Calculation of the relative rate of decay for a molecule just inside the surface of a particle 5 μm in radius with a tangentially oriented transition moment.

Although only TM modes appear in the spectrum for a radially oriented dipole (Fig.5), turning the dipole so that it is tangent to the surface (θ=90^o) changes the spectrum profoundly, as is seen in Fig.6. Not only do TM modes appear, but additional Transverse Electric (TE) modes arise, and the rate of decay, although depressed off resonance, as in Fig.5, is not as greatly effected. These differences between the spectra for the perpendicular vs. parallel molecular orientations (i.e. Fig.5 vs. Fig.6) provide a possible tool for determining molecular surface conformation.

III. C. The Relationship to Quantum Principles

The above approach of calculating how an excited state behaves in a microstructure by computing the reaction of an oscillating dipole to the scattered field (Eqn.2), may seem naive, since it contains little quantum mechanical detail. However, quantum mechanics has influenced our approach. Transition dipole moments are predicted by quantum mechanics and if the expectation of the dipole operator is treated by time dependent perturbation theory (using the scattered field as the perturbation), the resulting dynamical equations are found to have the same form as Eqn.2.

Unfortunately our mathematical model does not provide a mental picture of why the enhanced effects which we observe occur so predominantly in microdroplets and not in centimeter scale vessels. Although numerical calculations of the size dependence can be made using our model, the reason for the size dependence is obscured by the complexity of the mathematics. So why is something as small as a microdroplet so much different from a centimeter sized droplet?

Here we have to ask why emission occurs at all. The knowledge gained in a quantum chemistry course does not take one far. In such a course we calculate the properties of "stationary states!" Not surprisingly, the answer lies elsewhere. It is contained in the quantization of the vacuum field.

Spaces containing no atoms or molecules are not empty, they are teeming with fluctuations. Just as a harmonic oscillator cannot be stilled by freezing it to absolute zero, the vacuum constantly creates and annihilates photons. This activity is what drives electronically excited states to their death. This leaves $\hbar\omega/2$ of energy in each mode, where ω is the frequency of the confined light. This fluctuating energy

generates an electric field $\sim\sqrt{\hbar\omega/(2\varepsilon V_m)}$ where V_m is the volume of such a mode. Considering this $(V_m)^{-1/2}$ dependence alone, the electric field in such a mode will grow as the volume of the vessel confining the fluctuations decreases. If we consider the mode volume to be the volume of a sphere, the fluctuating field in a 10μm sphere will be ~30,000x the associated field in a 1 cm size sphere. So quantum mechanics or more correctly CQED delivers a flash of insight for answering our question, but it is a excessively complicated when it comes to its application to molecular systems in condensed matter.

IV. EXPERIMENTAL APPROACH

To test the radiation reaction theory as applied to spontaneous emission (Eqns. 2&7) we could perform experiments on typical hydrosols or aerosols, however the polydispersity of such a sample would certainly hide features such as those predicted in Figs. 5&6. Unfortunately no polydisperse sample would be tight enough in size distribution. Instead we will take a more classical approach and attempt to obtain a spectrum on a single spherical microdroplet. This requires a suspension technique, for certainly the stress and wetting effects associated with a surface will distort the droplet.

We turn to a levitation approach in which we can overcome the natural tendency for drift which is inherent in a Millikan chamber. The device, described in Section IV.A, uses an oscillating field (AC) to produce a time averaged trap and a constant DC field for levitation. Following this, we turn our attention in Section IV.B to aspects of molecular design, and offer explanation for the choices of particular surfactant chromophores. These results become the basis for the fabrication of a well defined systems (Section IV.C).

As we will see, by taking polarization selective images from a levitated particle we obtain strong evidence of chromophore isolation and orientation at the surface. Monolayer formation is signaled by an abrupt change in the evaporation rate. This measurement requires tracking the particle mass by using the levitator as a picobalance (Section IV.C.ii). Also presented is a puzzling effect in transport through a monolayer which shows discrete steps in the measured evaporation rate.

In Section V, spectra are displayed with and without the addition of an optically inert surfactant which acts as a supporting scaffold for the chromophores.

Finally these spectra are compared with the theory (Section V.B) developed previously in Section III.B describing the orientational dependence of the surface enhanced emission rate. We will show that the comparison between theory and experiment provide not only a test of theory, but a novel tool for evaluating aspects of molecular conformation at a liquid interface.

IV.A. Evolution of the Aerosol Particle Microscope Spectrometer (APMS)

IV. A.i. History of the Aerosol Particle Microscope (APM)

Crucial to the progress of experimental work has always been the limitations of observation. The ever evolving field of science necessitates the development of devices enabling progress. Through many years of research at the Microparticle Photophysics Laboratory several instruments have been invented for the generation and isolation of microdroplets. For microdroplet generation, the laboratory invented the "picopipette".[15] With it picoliter droplets could be generated and charged. For optical investigations of suspended droplets the laboratory recently developed an Aerosol Particle Microscope (APM).[16] It consists of a microscope which peers into an Electrodynamic Levitator Trap. With it, images can be taken of a suspended microdroplet in either elastic or inelastic scattered light, while the particle is illuminated from the side ("side-lit") or back ("back-lit"). Fig. 7 shows the side-lit "image" of a particle ~10μm in radius, taken in elastic scattering.

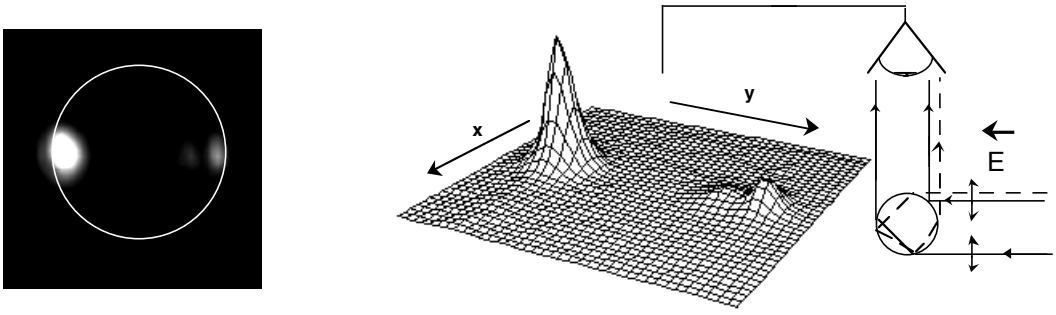

Fig.7 Image of a side-lit particle, topograph showing relative intensities, and a "glare beam" rationale. The white circle has been drawn in to show the droplet circumference.

This is know as a "glare spot" image.[17] The white outline in Fig.7 has been "sketched in" to show the circumference of the droplet. All that one actually "sees" are three pronounced dots of light. A rationale for their existence is sketched in at the right. The outer most pair come from diametrically opposed edges of the particle. By calibrating the CCD camera that records the image one can estimate the particle size. This method was used throughout this research for preliminary size determinations. The accuracy is limited to the width of a CCD pixel and the resolution of the microscope (depending on the size of a particle, ~1%). The remaining challenge was to develop a means for recording spectra of the inelastically scattered light as well as images. Fig.8 depicts the current instrument setup as it has evolved during the last year.

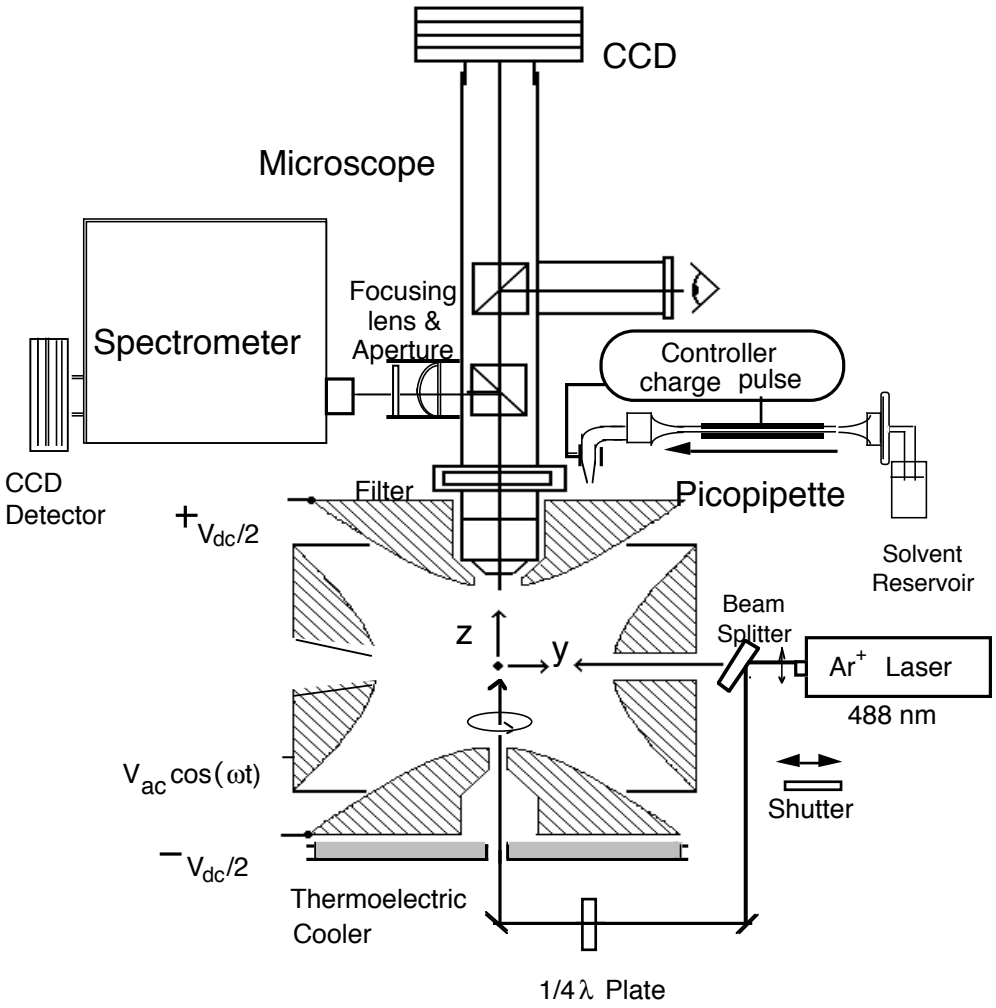

Fig.8 The Aerosol Particle Microscope Spectrometer

IV. A.ii. Development of the APMS

To capture fluorescence spectra from the microdroplets, a spectrometer that could view luminescence emitted at 90º to the incident beam was needed. With the addition of a sliding mirror to re-direct the emitted fluorescence through an efficient optical train (monochromator, CCD detector, and computer) an emission spectra could be measured and analyzed. Furthermore, due to the similarities in scattering phenomena, the same device enabled the examination of Raman signals. This required additional spatial filtering, and the use of a holographic notch filter for rejecting elastic scattered light.

Prior to taking spectra, the wavelength scale of the spectrometer was calibrated using a low pressure Hg lamp. The spectrometer consisted of a 1/4 M Jarrell-Ash monochromator (F/3.5) and a CCD detector. The detector, an astrophysical imaging device from the Santa Barbara Instruments Group (SBIG model ST-6), has 750 pixels across its width. In conjunction with a 1200 lines/mm grating in the monochromator, each pixel was found to cover a spectral width 0.379 Å (Fig.9).

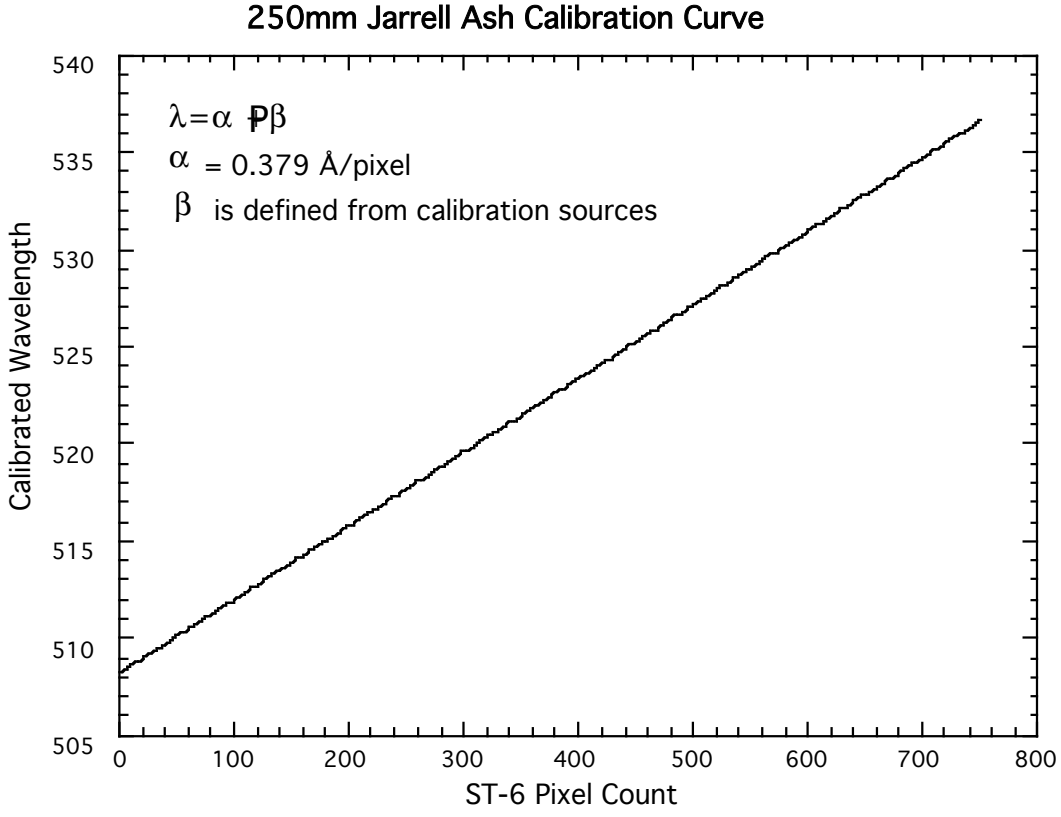

Fig. 9 Calibration of Jarrell Ash 250mm Spectrometer

Later spectra were obtained from a similar setup however the monochromator was changed to a 300 mm (Czerny-Turner) Acton Research Corporation SpectraPro 300i (F/4). Unlike the sine drive design of the of the Jarrell Ash, calibration of the Acton (driven by a computer interfaced stepper motor) was not constant throughout the grating tilt. Instead, using several sources, the linear dispersion could be found as a function of measured wavelength (Fig.10). For our particular system of interest emission occurs at ~519 nm, therefore the linear dispersion used was 0.0152 nm/pixel.

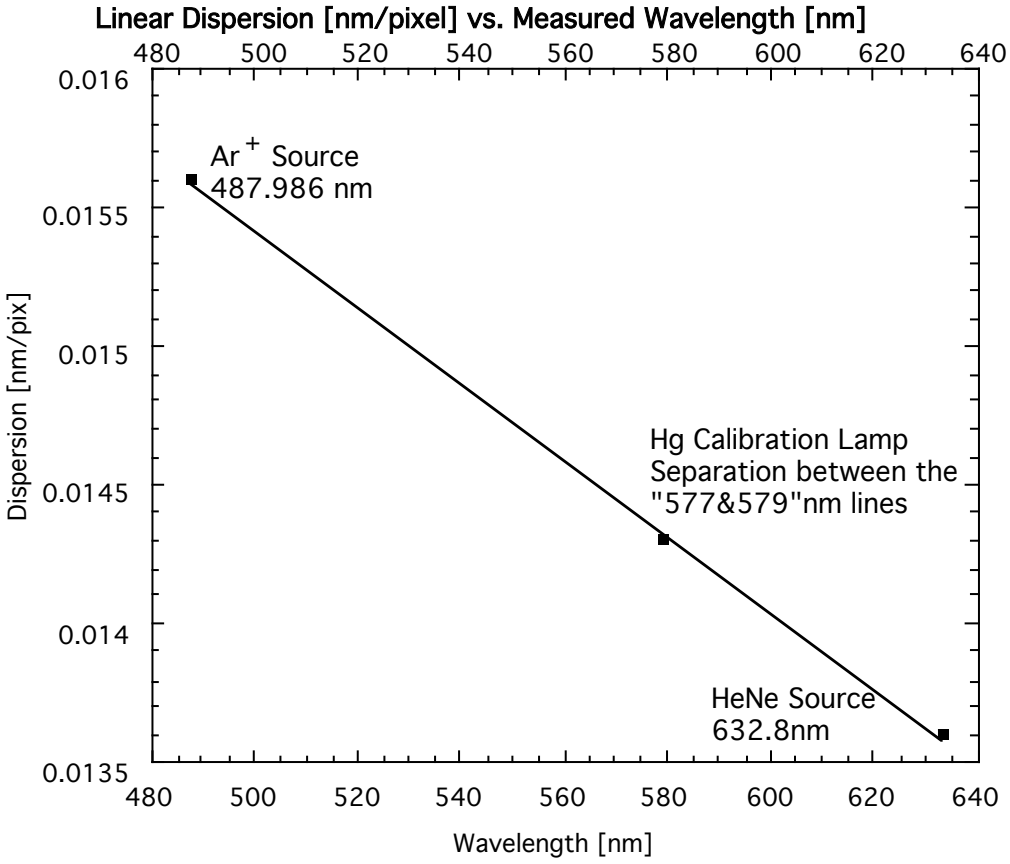

Fig.10 Calibration of the Acton SpectraPro 300i Monochromator

IV. B. Work on Surface Active Species

We have written the semiclassical theory for the spontaneous emission from molecules just below the surface of the microdroplet in order to focus our thinking to a region where we could hope to place a molecule. The idea is to use surfactant dye

molecules with the hope that they will not only localize at the surface but also orient. Such an experimental arrangement should provide a critical test of theory.

Surfactant layers are formed when the entropy of mixing is overcome and components separate due to immiscibility. If the dielectric bulk and chromophore are miscible, the chromophore should be anchored to the surface by attaching an immiscible molecular component. In our case, the solvent is glycerol, which is polar. Thus if a nonpolar segment, such as an aliphatic chain can be attached to a chromophore, the dye is pulled to the surface. The heterogeneity in composition can be detected through images taken of the system in fluorescence using the APMS (Fig.8).

To form the composite particle with chromophores at its surface a single picoliter size droplet of glycerol and methanol (2:1 ratio) containing a dilute chromophore [10^{-5}M and immiscible (i.e. surfactant) in glycerol], is injected into the levitator-trap by supplying an electrical pulse to the piezoelectric strips in the picopipette body. After being trapped, the methanol co-solvent evaporates rapidly, and the surfactant is driven to the surface of the droplet. Fig. 11 shows a typical image of a back-lit particle. A pronounced rim is observed, indicative of surface layer formation,[15] and central spot due to laser focusing.

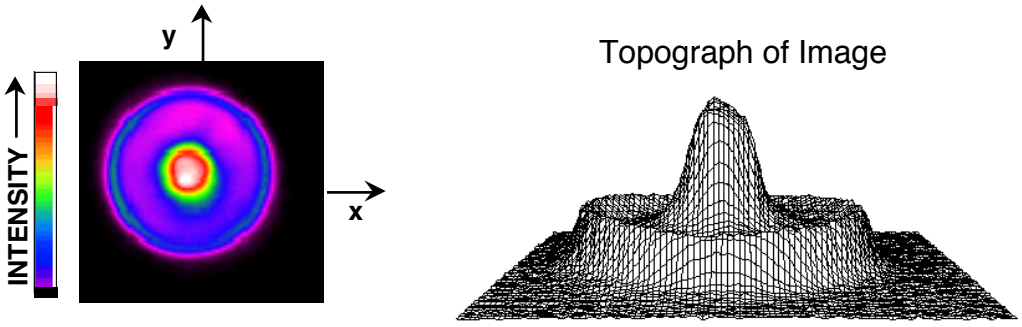

Fig.11 Sample Image of a back-lit droplet containing surfactant dye and a topograph of the image

IV.C. Oriented Molecular Systems on a Micro-droplet

IV.C.i Standard Surface Dyes

With the chromophores now confined to the surface, their position with relation to the bulk is known. However, we wish to investigate orientational effects. The topic requires additional confinement of the emission moment relative to the surface normal. Every chromophore possesses an emissive moment defined by its unique molecular orbital structure. Specific molecular architecture is used to further confine the chromophore by anchoring it within the surface plane.

In general, linear polyaromatic hydrocarbons typically have emissive moments defined along the long axis of the molecule. Likewise, a number of variant visible dyes, utilizing linear combinations of heteroatom aromatic rings and conjugated pi-bond systems possess well characterized moments along their long axes. One such family of dyes is known as the carbocyanine dyes (Fig. 12)

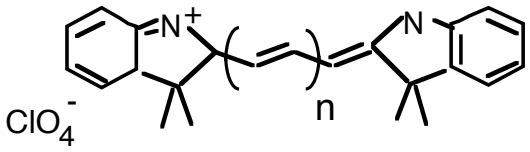

Fig.12 General structure of the Carbocyanine chromophore

Besides its desirable linearity, the structure provides one unique advantage. In its salt state, aliphatic chains of great length can be attached to both opposing nitrogens on either of the five membered hetero-rings, providing equal anchorage to each side. For our excitation wavelength (488nm), the appropriate chromophore was named 1,1'-dioctadecyl-3,3,3',3'-tetramethylindocarbocyanine perchlorate, or DiI(3) (D-282, Molecular Probes), where n=1 and aliphatic chains were 18 carbons in length. When diluted to an appropriate concentration (e.g. 10^{-5}M) to avoid self-association, the dye is isolated to the surface, as envisioned in Fig.13, The dual anchorage is expected to confine the long axis of the chromophore tangent to the surface of the sphere, or 90^{o} to the surface normal.

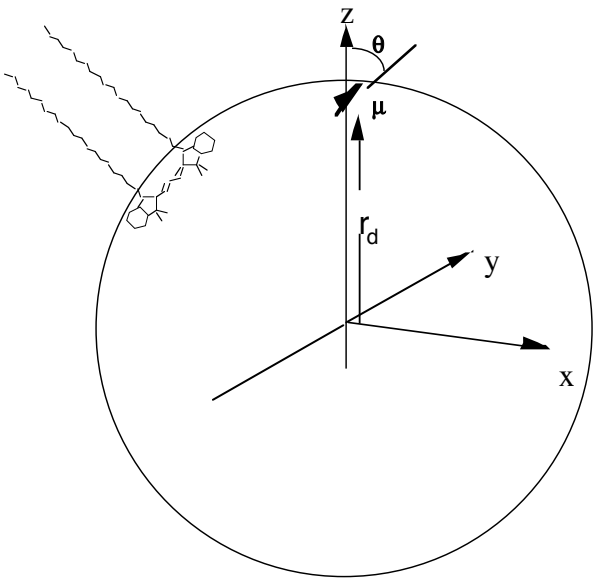

Fig.13 Schematic diagram of a single DiI(3) Molecule anchored at the surface of a microdroplet

To test whether moments are homogeneous or heterogeneously oriented within the surface, we recorded polarization selective back-lit images.[18,19] The particle is irradiated with circularly polarized radiation (488 nm) in order to eliminate any azimuthal bias. The resulting images taken in DiI(3) fluorescence, with and without a polarizer preceding the CCD, can be seen in Fig.14a and 14b, respectively.

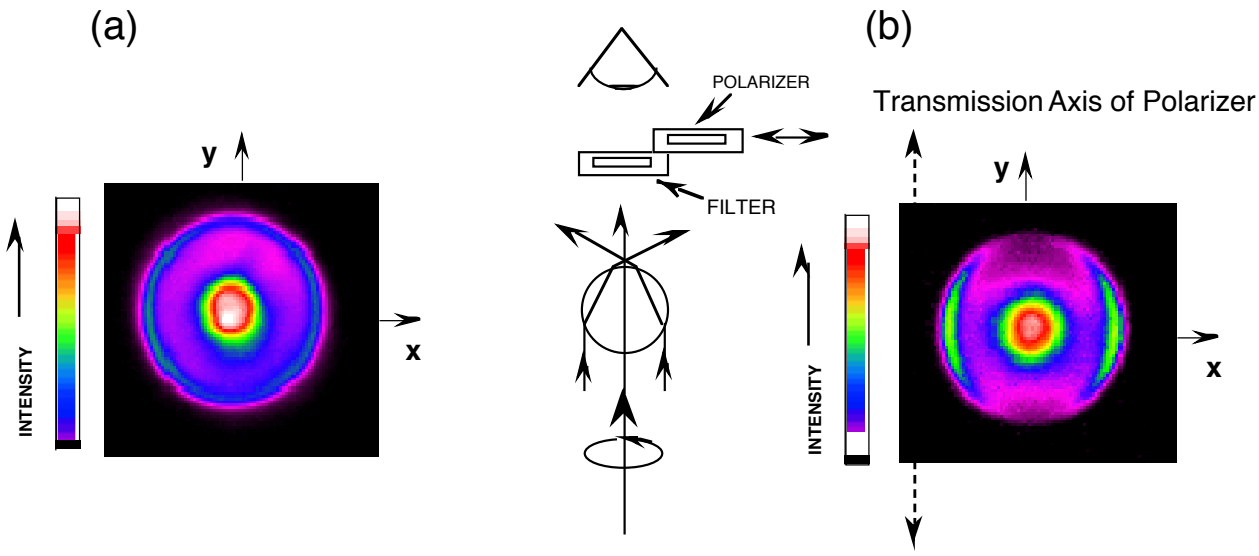

Fig.14 Images of a backlit DiI(3) surfactant in a glycerol droplet with (a) and without (b) a polarizer

Like the image of the surfactant in Fig. 11, we see a pronounced rim at the surface of the droplet, indicative of surface layer separation of the chromophore. However when the same droplet is imaged through a polarizing filter, parts of the rim vanish where the polarizer transmission axis is perpendicular to the surface boundary. We infer from this image that the transition moment of the surfactant emission moment perpendicular to the surface normal; parallel to the particle surface.

So, what results from a spectrum taken of the same DiI(3) droplet? Fig.15(a) shows a typical spectrum of a DiI(3) doped glycerol particle (10^{-6} M) estimated through glare spot separations to have a radius of 7.5+/- 0.2 μm.

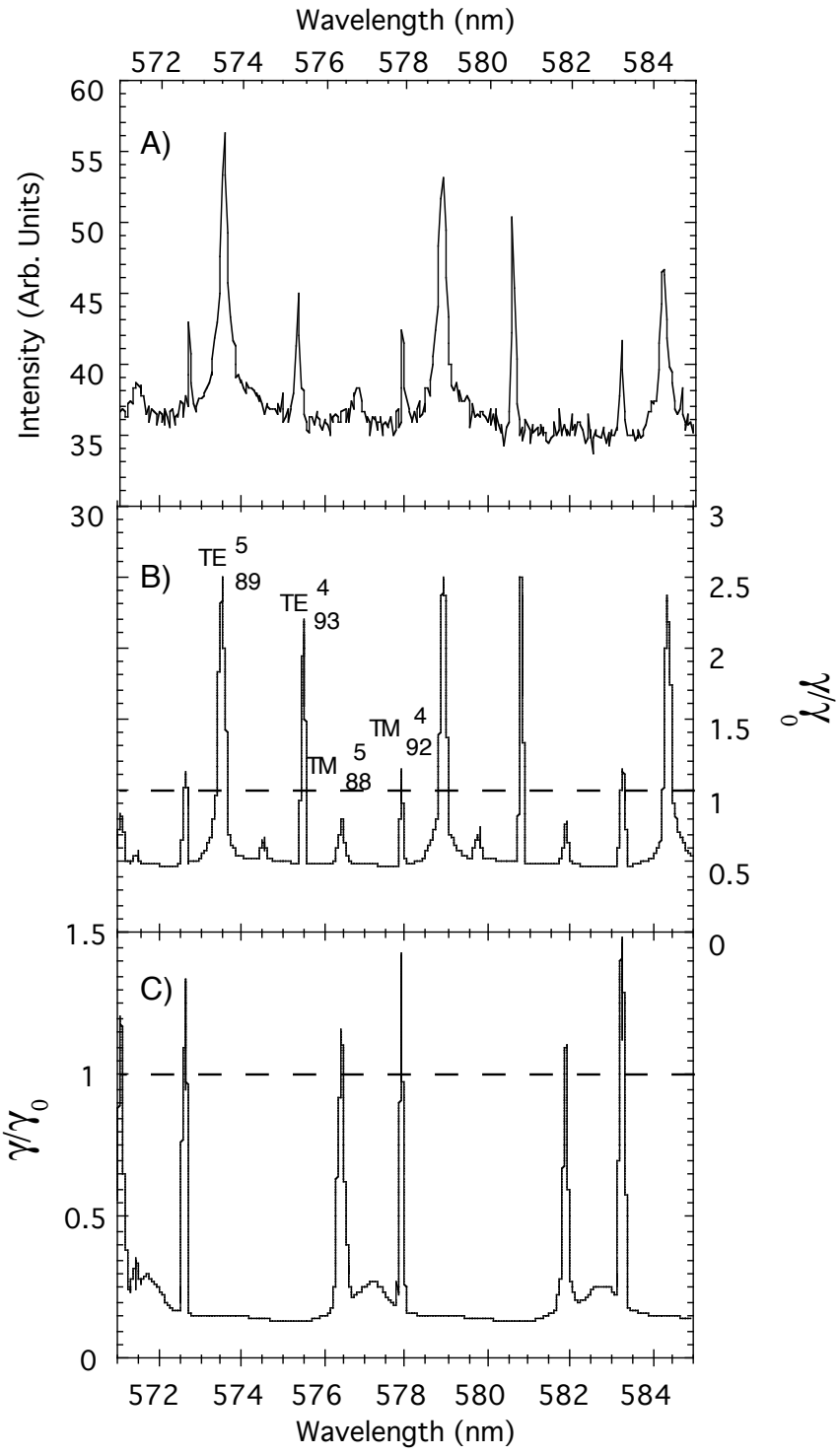

Fig.15 (A) Spectrum of a DiI(3) doped glycerol particle (10^{-6} M) approx. 7.5 +/- 0.2 μm in radius. Semiclassical calculation for a dipole tangent (B) or perpendicular (C) to the phase boundary in a particle 7.3656 μm in radius.

Although resonances have been measured on soluble dyes in the past, the spectrum in Fig. 15 (A) is distinct due to the variation in peak areas. For soluble dyes although peaks vary in width, the areas under them are essentially constant.[20] This is clearly not the case for the DiI(3) spectrum. The variation in peak areas is as much as a factor of 10. However this is what may be expected from an oriented dipole. In particular a dipole oriented tangent to the surface projects more strongly onto TE modes than TM modes as we have seen from our simulations (Figs. 5 and 6).

In Fig.15 (B) and Fig.15 (C) we show the semiclassically calculated spectra (Eqn.8) for a dipole tangent (B) and perpendicular (C) to the phase boundary in a particle 7.3656 μm in radius.[21] We see that the agreement between the experimental spectrum and tangent hypothesis [i.e. Fig.15 (B)] is good, and clearly shows that the TE modes are dominant. Interestingly a variation in size by as little as 0.0001 μm throws the agreement off. It is very clear from Fig.15 that the emission moment could not be perpendicular to the surface. Such a circumstance eliminates half of the resonances seen in Fig.15 (A). Clearly the perpendicular hypothesis is a severe case of mode selection (i.e. only TM modes are stimulated). To complete our understanding of the interrelationship between theory and experiment we would like to construct this perpendicular case experimentally.

Unfortunately, the reality is that most linear or planar molecules are forced to orient tangentially to the surface due to the confinement of surface energy. The challenge is to design a system in which the emission moment orientation is varied such that the spectral change is evident. Ideally, if the same chromophore could assume multiple orientations through a fixed architecture, the model could be tested to fit the spectra of a well defined system. The solution lies in molecular design of surfaces, particularly monolayers that can act as optically inert support structures.

IV.C.ii Molecular Architecture

IV.C.ii.a Building a Monolayer on a Microdroplet

Traditionally, any region separating two phases is defined as an interface. In the case of an aerosol micro-droplet, a separation exists between the liquid bulk and its gaseous surroundings. Even though this region comprises a minority of molecules, it profoundly effects the existence of such a particle. Evaporation is restricted by the surface layer, and this region is the conduit though which all

molecules must pass in order to react with the bulk. In this section we will outline our method for building molecular monolayers.

In attempting to form a monolayer on a microdroplet, it would be convenient if we can use information derived from monolayers formed on a flat interface. In this respect there are a great many experiments using Langmuir-Blodgett technique. Of course, our system differs. The surface of a droplet is curved and the interior of a droplet is limited.

For a microdroplet (radius, a ~10μm) the curved surface should present little difficulty in arriving at an estimate of the concentration required to build a monolayer. Energetic considerations dictate the volume taken up by a molecule at the surface, v_o, is controlled by the ratio of molecular length, l, to droplet radius, a, through the relation[22]

$$v_o = \Sigma_o \, l \, [1 + (l/a) + (1/3)(l/a)^2] \qquad (12)$$

where Σ_o is the surface area per molecule on a planar interface. Since a microdroplet is ~ 100,000 Å (i.e. 10μm) in radius and a surfactant molecule is only ~10Å in length, the ratio l /a may be neglected in Eqn.12, and $v_o \approx \Sigma_o \, l$, the volume on a planar interface.

The easiest way a generate the surface layer is to dissolve partially miscible surfactants within the droplet. By using insoluble aliphatic "tails" on acidic "heads," the entropy of mixing is overcome, causing the surfactant molecules to be driven to the surface. As monolayer formation is also dependent on packing the molecules to an adequate surface pressure, a mechanism for compression must be designed. A natural solution is the addition of a volatile co-solvent. Thus, after the droplet is trapped, the co-solvent begins to evaporate, subsequently reducing the volume as well as surface area.

The concentration of surfactant within the droplet should be sufficient to cover the final surface area. Consequently, the average concentration of surfactant, ρ, times the volume of the droplet should be equal to the surface concentration, $1/\Sigma_o$ times the droplet area. On this basis, the concentration in the droplet would be $3/a\Sigma_o$, where a is the droplet radius. As the concentration is reduced, liquid layers are expected to form followed by gaseous layers in the dilute case. If instead, the concentration of surfactant is too high on the surface, the monolayer will begin to wrinkle and fold to relieve excess strain.

IV.C.ii.b Monolayer Design for Specific Chromophore Orientation

Our interest in what follows is to provide a further test of theory by designing a molecular system in which the emission moment has a large out of surface component.

Designing a chemical system with a perpendicularly oriented chromophore entails two major concerns. First, the transition moment of the chromophore must be well defined relative to its molecular structure. Second, a supporting structure must orient the transition moment perpendicular to the surface.

The microdroplet will be generated using a three component system as described in the last section. In each case the substrate will be a glycerol liquid surface. Glycerol is ideal due to its low vapor pressure (~1 mTorr) and inertness to other components. The experiment can be conveniently run over several hours in a dry atmosphere (i.e. diffusion limited transport) without a significant change in particle size.

As the surfactant molecules are compressed on the glycerol surface with the evaporation of the co-solvent, a layer will begin to form. The ever shrinking size of the micro-droplet is analogous to the gate in a traditional Langmuir-Blodgett trough. In a sense, the evaporating microdroplet becomes a microscopic spherical Langmuir-Blodgett trough.

A simple example of surface active molecules is soap on water. Soap is typically composed of fatty acids. The aliphatic chain is nonpolar while the acidic head is polar. As like dissolves like, the polar head anchors the molecule into the water and the nonpolar tail remains at the interface. Provided the density of chains is sufficiently saturated, the tails will pack tightly above the heads creating a monolayer. The hope is that a similar behavior will be observed on glycerol.

Quantitatively, the co-solvent can be added at a sufficient concentration, so that when it evaporates the particle's size is appropriate for monolayer formation. The co-solvent also serves a dual-purpose in the droplet generation process by lowering the viscosity of the primary solution. To date, we have not been able to eject pure glycerol droplets with our picopipette.

IV.C.ii.c The BODIPY Fluorophore and Heterogeneous Packing

To select an appropriate dye one first considers the spectral characteristics of the chromophore. A trademark membrane dye of Molecular Probes Inc. (D3826),

BODIPY, possesses not only ideal excitation properties for the Ar^+ excitation line at 488 nm, but is synthesized to include various lengths of aliphatic chains on either side of the symmetrical chromophore (Fig.16). Additionally, on the end of one tail exists a carboxylic acid group for anchoring to the polar solvent. Thus, the chromophore structure does not differ greatly from common fatty acids that are frequently used in monolayers (e.g. stearic acid). The combination of BODIPY and stearic acid results in a heterogenous monolayer which aside from the chromophore, is nearly homogeneous (Fig.16).

Linear dichroism measurements reveal that BODIPY has a well characterized transition moment.[23] The electronic dipole of the S_0 -->S_1 transition is polarized along the long axis of the chromophore (Fig.16). Therefore, provided the hydrophobic tail of the BODIPY is similar in length to that of the fatty acid and the emission moment lies in approximately the same direction as the absorption moment, the packing, despite tilting from chain entanglements, could leave the emission moment practically perpendicular to the surface. Additional complications imposed by the curvature of the surface, are negligible, as explained previously (Eqn.12).

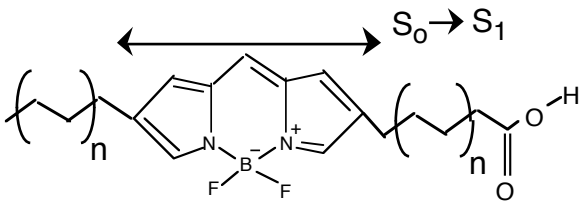

Fig.16 BODIPY With Variable Length Carbon Chains and Acidic Head

To create the appropriate scaffolding we require that the volume concentration of surfactant, ρ, times the volume of the droplet be equal to the surface concentration, $1/\Sigma_o$, times the droplet area. The resulting surfactant concentration in the droplet then becomes $3/a\Sigma_o$. Σ_o as defined for a fatty acid of 18 carbons (stearic) has been found to equal ~ 0.22 $nm^2/molecule$.[24] Fig.17 shows the calculated volume concentration (Eqn.12) of stearic acid vs. microdroplet radius
for monolayer formation where surface area per molecule in a monolayer equals $\Sigma_o \sim 0.22 nm^2/molecule$.

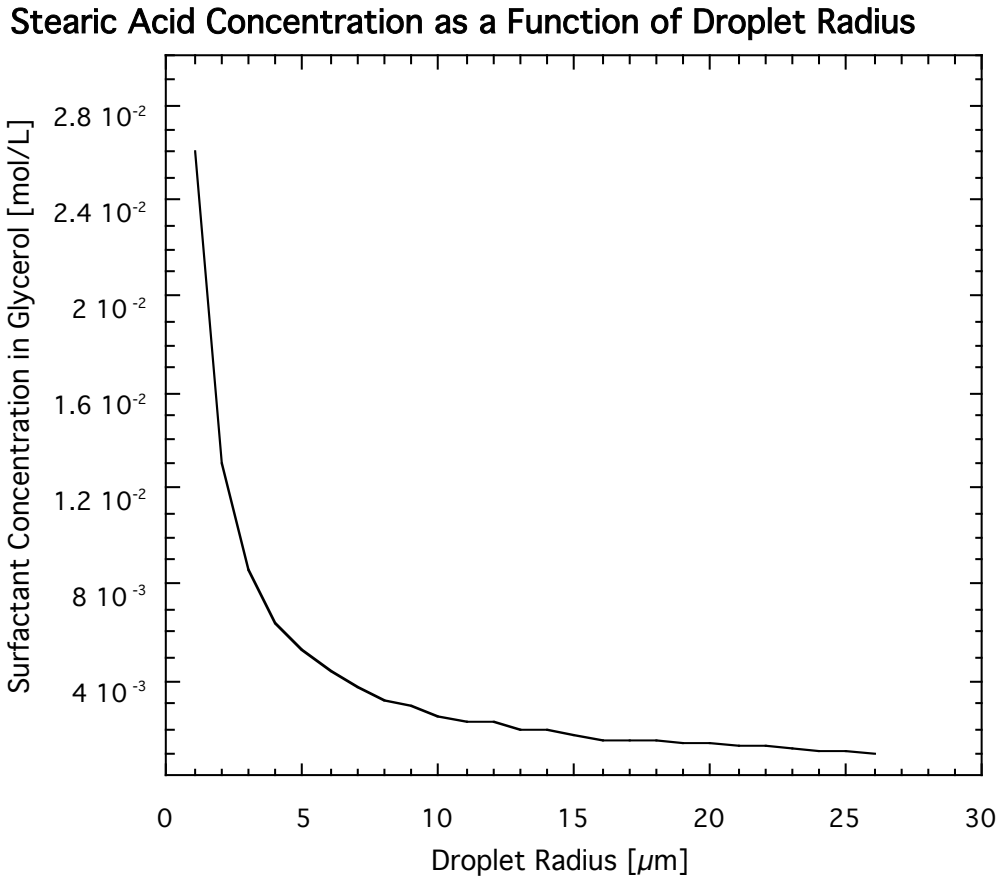

Fig.17 Optimum surfactant concentration for formation of a single monolayer on a microdroplet of given radius

For particle radii of 5 and 10μm the associated concentrations of stearic acid are 4 x 10^{-3} mol/L and 3 x 10^{-3} mol/L, respectively. To avoid self association of the dye at the surface, BODIPY's concentration was diluted by an order of magnitude to 10^{-4} mol/L. However, the supporting fatty acid concentration was chosen to remain at the calculated order of 10^{-3} mol/L.

The BODIPY molecule possessing the shortest carboxylic anchor (5-decyl-4, 4-difluoro-4-bora-3a, 4a-diaza-s-indacene-3-proprionic acid, or C_{10}BODIPYC_3) was chosen to assure that the chromophore was close to the bulk interface.

IV.C.ii.d The Evaporation of a Microdroplet

Although the influence of the monolayer formation should be evident spectrally, additional physical measurements can be made to confirm the existence of surface assembly. The solution came from the investigation of glycerol diffusion

from the droplet into the surrounding atmosphere. In diffusion limited processes, the surface area of a droplet decreases linearly with time. However one would expect that the formation of a monolayer at the evaporation interface would act as a partial barrier to evaporation. Fortunately, by its very nature, the levitator trap acts like an "pico-balance".[25] Thus if the decreasing size can be understood in terms of balancing voltage, physical measurement of the droplet evaporation can be recorded.

Let us investigate the diffusion limited evaporation process for a microdroplet levitated in a gaseous environment. For a full derivation see Appendix I.

Since the mean free path of gas molecules at 1 atm. is ~ 0.06 μm and the droplets we are dealing with are ~ 10μm in radius, evaporation of glycerol from a droplet will be diffusion limited. In this regime one can show (Appendix I) that the particle will decrease its surface area (alternative radius squared) linearly with time is accordance with

$$\left(\frac{a}{a_o}\right)^2 = 1 - \frac{2\,D\left(\frac{P_S\,M_S}{RT}\right)}{\rho\,a_o^2}\left(t - t_o\right) \qquad (13)$$

where D is the diffusion coefficient of glycerol through air, P_s is the vapor pressure of glycerol at absolute temperature T, and ρ is the mass density of glycerol. Instead of monitoring the size of the droplet we will use the levitator-trap as a "picobalance" and monitor the levitation voltage, which is proportional to the droplet's mass. This convenient relationship results from the fact that evaporation of a polar droplet is charge preserving, as a consequence of the high solvation energy associated with an ion in the liquid. Consequently Eqn.13 becomes

$$\left(\frac{V_{dc}(t)}{V_{dc}(0)}\right)^{\frac{2}{3}} = 1 - \frac{2\,D\left(\frac{P_S\,M_S}{RT}\right)}{\rho\,a_o^2}\left(t - t_o\right) \qquad (14)$$

We have performed several evaporation experiments on our microdroplets. These experiments purge glycerol from the air at a large distance from the droplet by using a slow flow of pure N_2 gas. The experiments agree in form with Eqn.14. For a 10μm homogeneous droplet of glycerol $V_{dc}^{2/3}$ decreases linearly with time (Fig.18). The data was taken at 24^{o}C on a particle with an initial diameter of 20μm. The slope

of the line through the data is -3.65×10^{-5} sec^{-1}. In an attempt to duplicate the data, another particle was suspended however its size was somewhat smaller (a~8μm), and therefore from Eqn.14 we would expect the evaporation to occur more quickly. The data demonstrates exquisite sensitivity to the size change accompanying evaporation. Indeed, Fig.18 shows a snippet of the 8μm evaporation curve indicating a slope of -5.59×10^{-5} sec^{-1}. The expectation from Eqn.14 is that this slope should be larger by a ratio of $(20/16)^2$ corresponding to a difference in initial droplet size. If we divide the slope of the 8μm droplet by this factor, we get -3.58×10^{-5}sec^{-1} -- in good agreement with our previous measurement of -3.65×10^{-5} sec^{-1}.

One can use this data to determine the vapor pressure of the droplet. The slope for the 10μm drop in Fig. 18 is equivalent to a rate of change of radius of -5.6 Å/sec. By using handbook[26] values for the other parameters: D = 0.26 cm^2/sec, M_S = 92.09 g/mol, and ρ = 1.26 g/cm^3, the vapor pressure P_S is found to be 2.40×10^{-6} atm. This number is in good agreement with the vapor pressure of pure glycerol. [26]

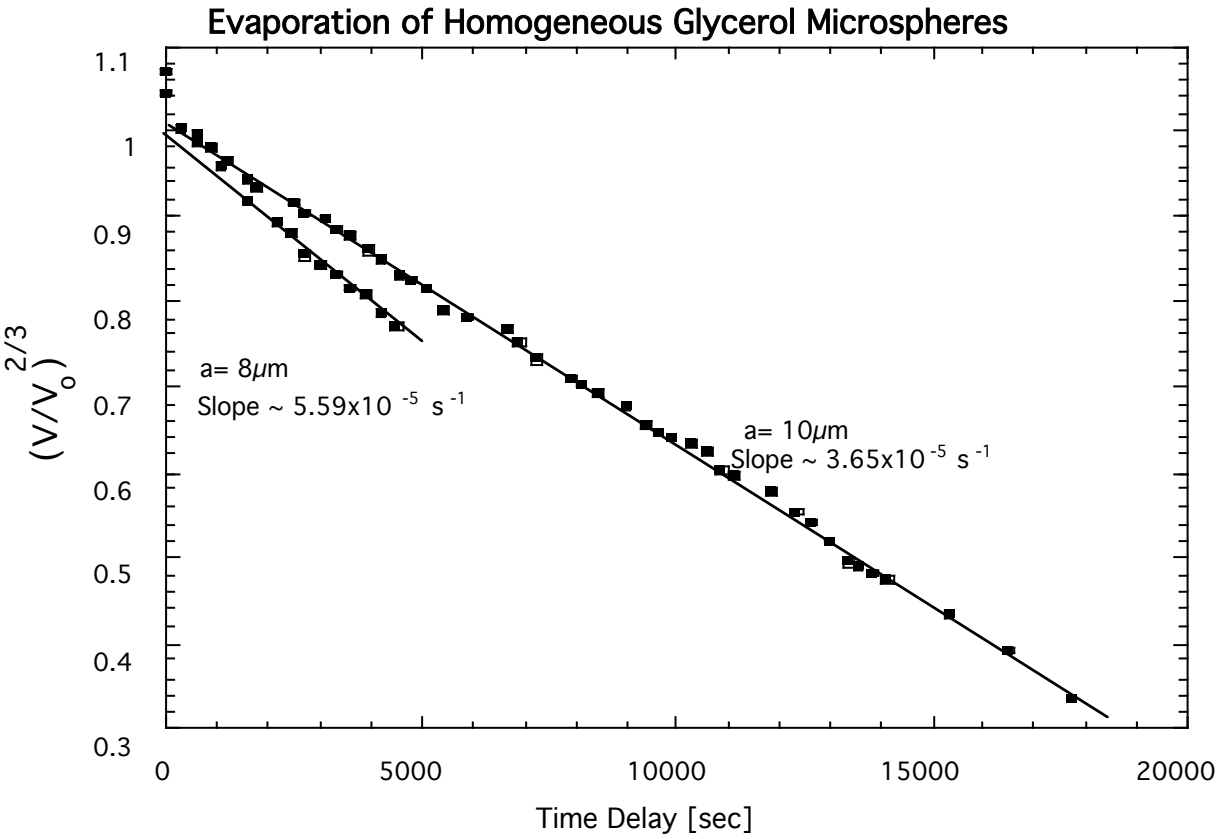

Fig.18 The evaporation of Glycerol Droplets of varying Initial Size

It is interesting to compare the results in Fig.18 with measurements on a stearate coated droplet (Fig.19). Like the measurements on pure glycerol, the initial slope is linear. However the profound change in slope, as well as the steps in voltage, suggest a more complex mechanism.

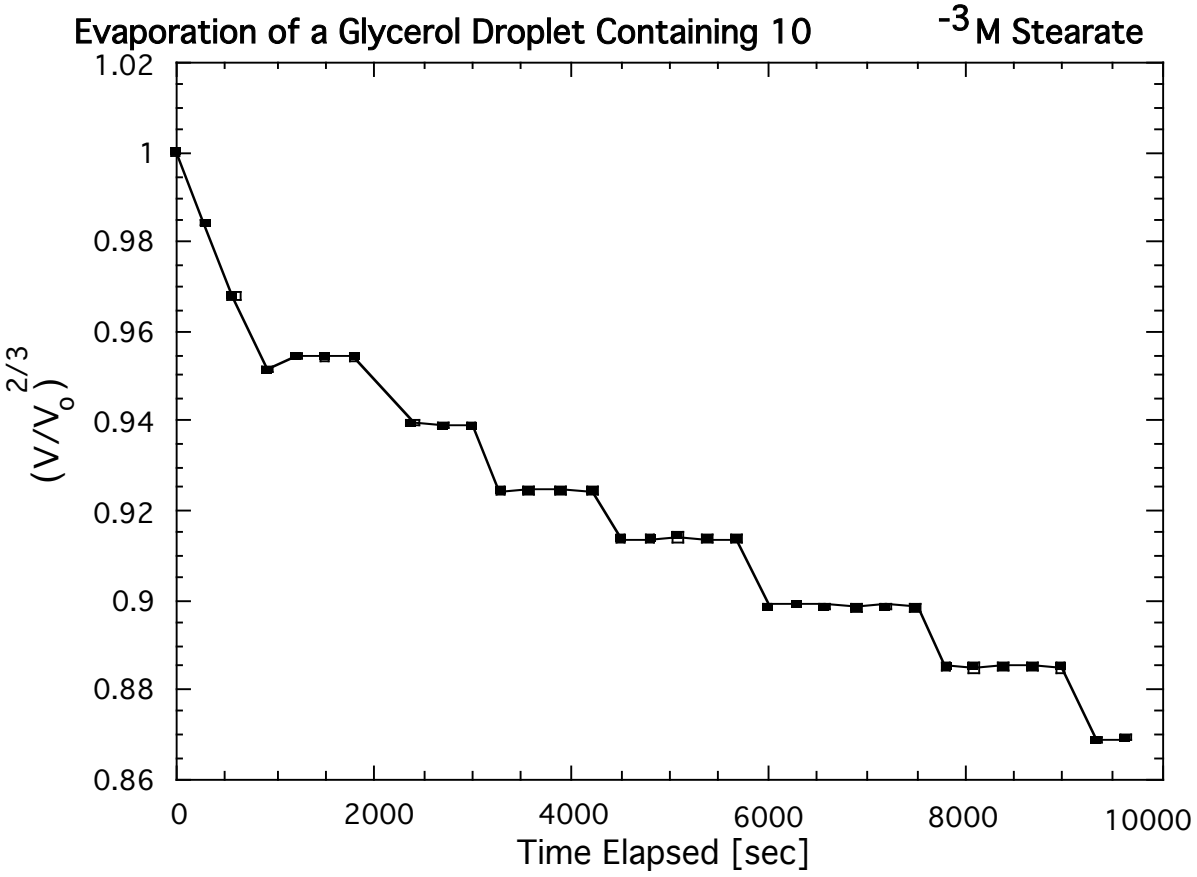

Fig.19 Evaporation of a Glycerol Microsphere with Stearate of Radius~8μm

To confirm the existence of the staircase, droplets of similar size were observed with and without the addition of a monolayer component (sodium stearate). For both cases the initial evaporation of glycerol was identical in slope until the evaporation essentially terminated and the staircase began. The results are shown in Fig.20.

One possibility for an abrupt change in levitation voltage would be an abrupt change in charge. However, this is unlikely for the staircase shown in Figs. 19 and 20. An abrupt change in charge may be necessary to relieve surface stress caused by an excess charge. However, under such a circumstance the levitation voltage would increase. Therefore, the more likely origin of the steps is a changing barrier to evaporation at the surface. This could be a result of a 2D solid to liquid phase

transition or the appearance of cracks in the surface. Cracks may be the way in which the two-dimensional layer accommodates to a changing curvature as the particle evaporates.

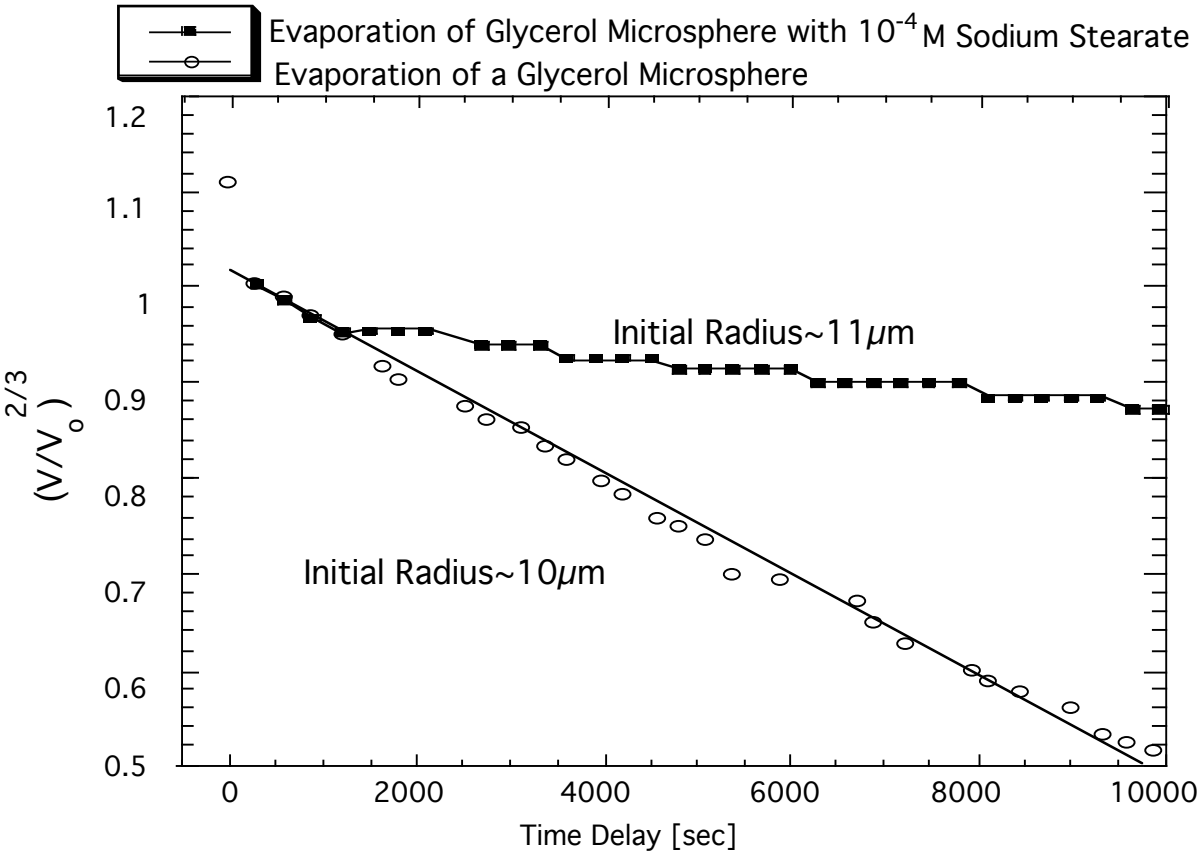

Fig. 20 Evaporation of a Glycerol Microsphere Compared to a Glycerol Microsphere of Similar Size Containing Stearic Acid of Similar Size

V. Spectroscopy Results

V.A. BODIPY with and without Monolayer Support

First, spectra were taken for a dilute impurity layer ($3x10^{-4}$ M BODIPY surfactant). Fig.21 shows the result for a particle ~ 7.6 μm in radius. It has five peaks per period.

In contrast, Fig.22 shows the spectrum taken on a particle ~ 7.5 μm in radius, but containing both BODIPY surfactant at $3x10^{-4}$ M and sodium stearate at $3x10^{-3}$M (i.e. at the critical concentration for monolayer formation, see Fig.17). The contrast with the unsupported case (Fig.21) is clear. Now there are only three peaks per period. The difference in the number of peaks per period is odd since

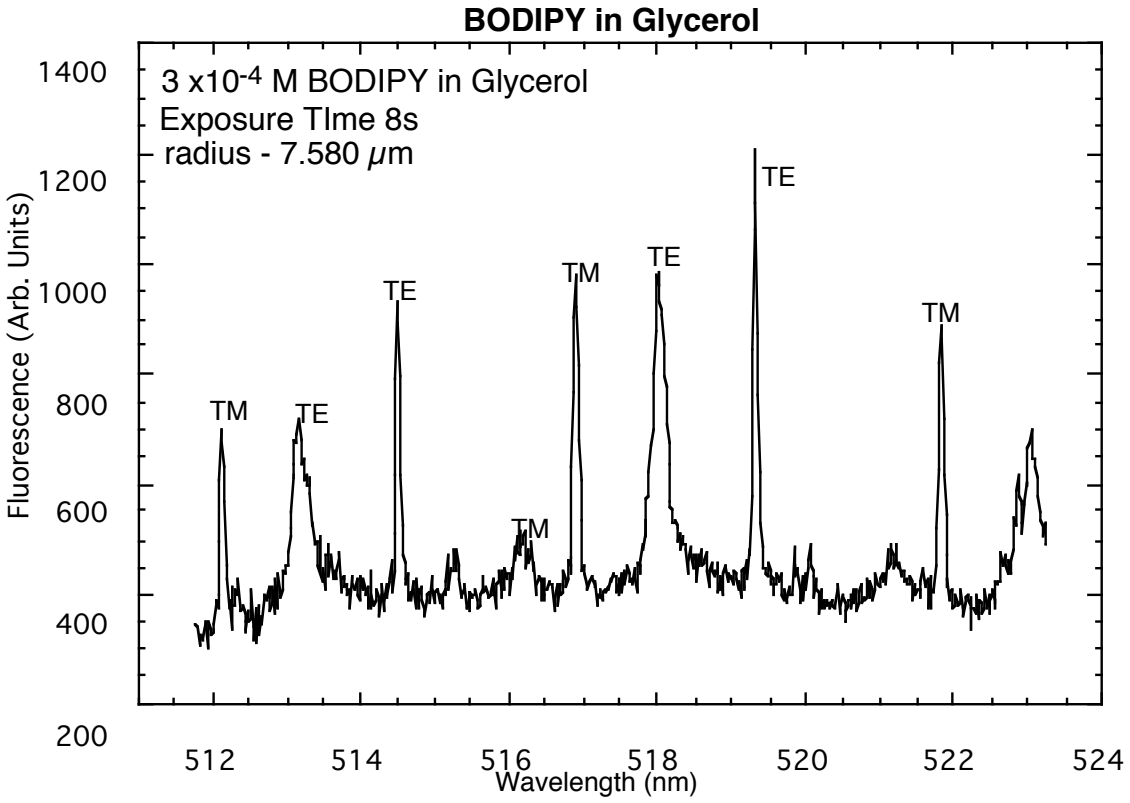

Fig.21/22 Spectra of BODIPY Doped Particlesof Radius~7.6 μm and 7.5μm Respectively

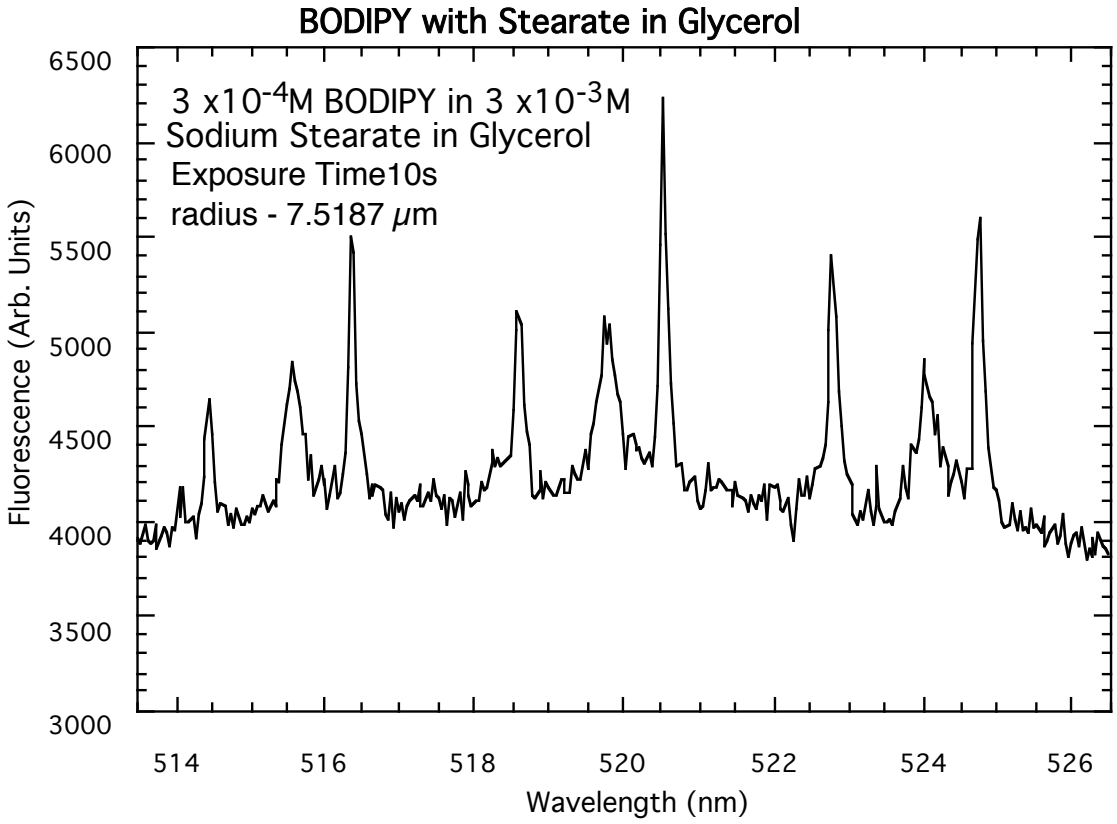

particles having similar sizes should have similar numbers of apparent resonances per period. Clearly the supported chromophores excite fewer resonances in the particle. A similar situation occurred in our simulations(Figs. 5 and 6). It is likely that this effect is the result of stimulation by a radially oriented dipole moment. A likely hypothetical structure consistent with this conjecture is shown in Fig.23. In constructing this figure we have supposed that the chain length of stearic acid is sufficient to support the entire protruding length of the chromophore surfactant. On this basis it appears that the BODIPY surfactant may be partially miscible. We will re-explore this possibility when we look at the correspondence between our spectral theory and experiment (Sec. V.B.).

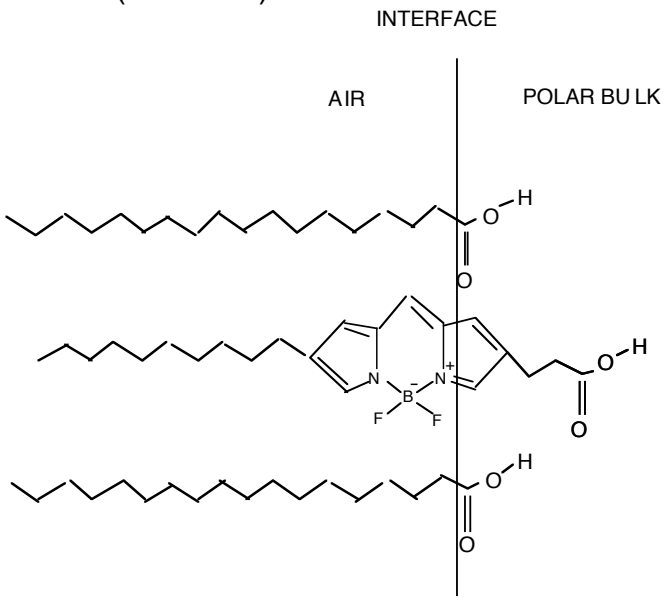

Fig.23 C_{10}BODIPY C_3 between two stearic acid ($C_{18}O_2H_{36}$) chains at an interface

It should be noted that the density of points per spectra is dependent on the spectrometer used. Fig.21 was taken with the 300mm Acton (1800G/mm Grating), whereas Fig.22 was captured on a 250mm Jarrell Ash (1200 G/mm Grating). Both setups are described in detail in the instrumental description of the experimental section (Sec.IV. A.ii.). Although the change in spectrometer produces a different resolution in each case, this difference is too small to have hidden peaks in Fig. 22 in comparison to Fig.21.

V.A.i. A Test of Chromophore Miscibilty

Other monolayer supporting structures were used along with the BODIPY surfactant chromophore. However in each case the resulting spectra showed more peaks per

period than in the sodium stearate case. Lauric acid (C_{10} tail like that of C_{10}BODIPY® C_3) is an interesting example as shown in Fig.24.

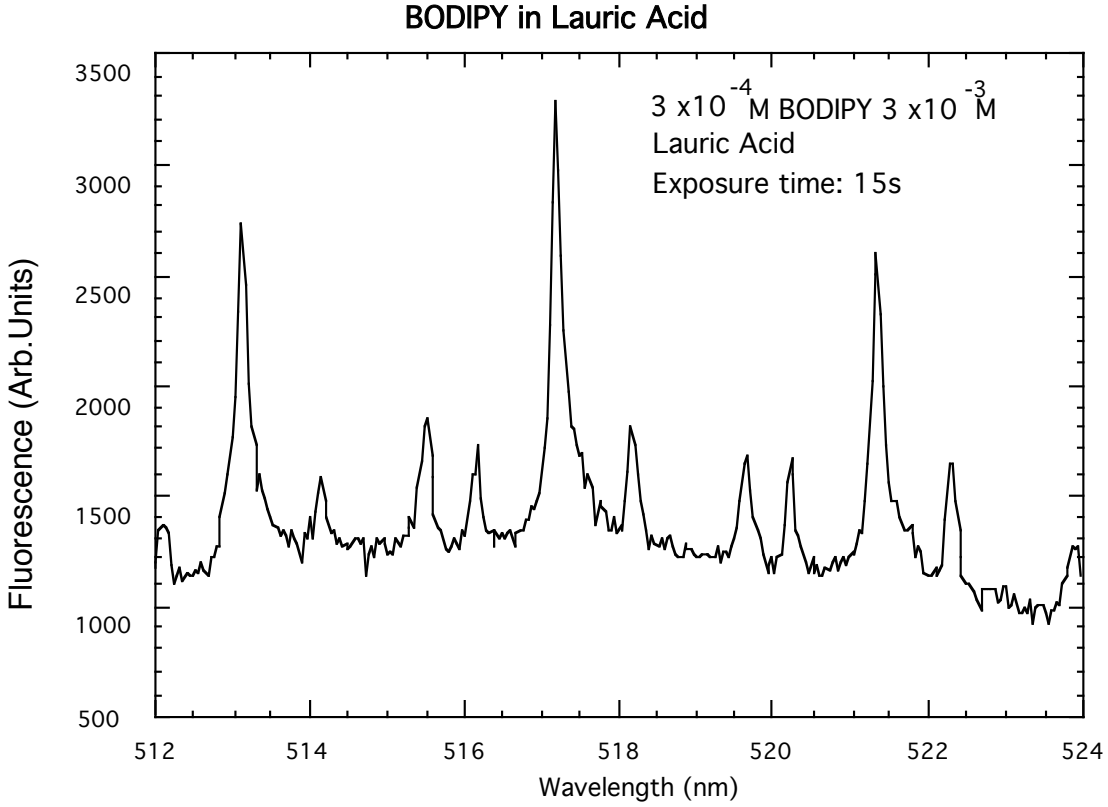

Fig.24 Spectra of C_{10}BODIPY C_3 ~7.5 μm Particle Radius

From the separation of resonances, we can see that the droplet is of comparable size (a ~ 7.5 μm) to those of Figs.21 & 22 However, there is one more resonance per period than in Fig.22, and the peak areas have been redistributed. This implies that the emissive moment has a component along the surface. It appears that the smaller chain length for Lauric acid cannot support the BODIPY surfactant chromophore as well as stearic acid. A likely scenario consistent with our original conjecture of partial miscibility is shown in Fig.25.

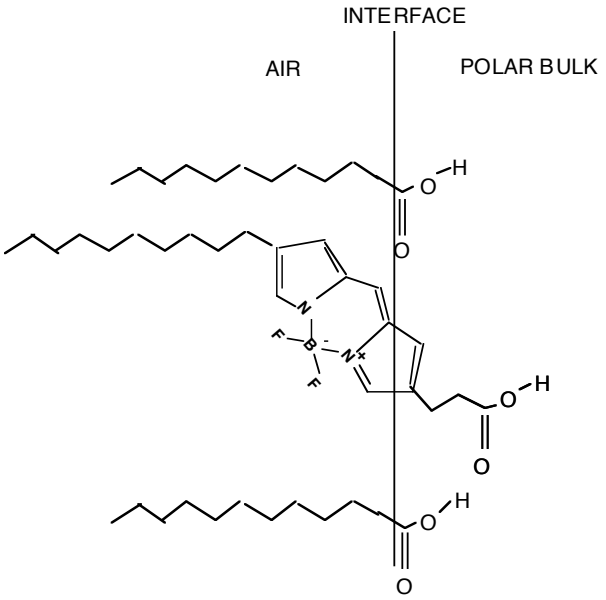

Fig.25 Possible Structure of BODIPY surfactant in a Lauric acid monolayer

If on the other hand, the chromophore had been completely miscible, one would expect the identically matched tail lengths to form an optimum homogeneously structured monolayer, resulting in a radial orientation in the emission moment (Fig.26).

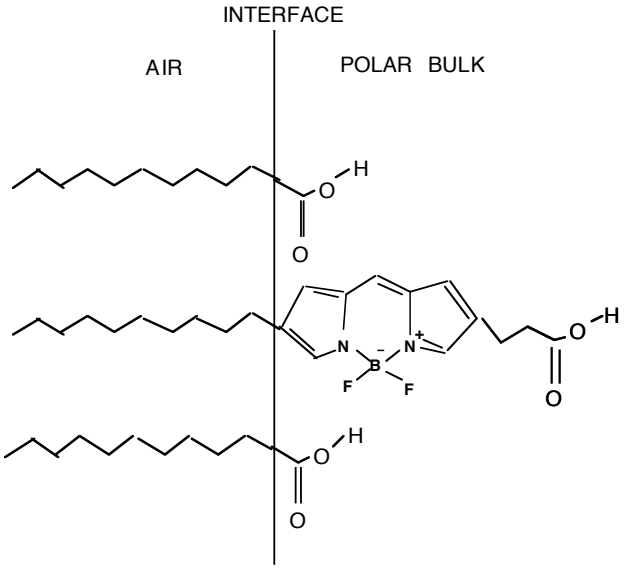

Fig.26 Hypothetical schematic of a Lauric acid monolayer where the BODIPY chromophore is completely miscible with the bulk.

Another possibility arises from the pH of a shorter hydrophobic chains allowing the monolayer to have an insufficient hydrophilic/hydrophobic balance, and therefore partially dissolving into the subphase.[24] Likewise, considerably longer tails cannot be used due to packing considerations of the monolayer, entanglements, and neutralization effects of the anchor head by a lengthy alkyl chain.

However to truly understand the origin of these differences, we should model spectra for droplets of similar size for the two extreme orientations to the normal. If indeed the supported spectra is without any TE resonances, then its emission moment is necessarily perpendicular. Due to the laborious calculations required to find position, strength, and width of each resonance as well as a convolution appropriate to the spectrometer's resolution, results are compiled through a computer program designed in Mathematica (Wolfram Research).

V. B. Spectral Modeling of the Normalized Rate of Emission by Surface Molecules

Figs. 21 and 22 provide the experimental results which we require for testing our theory of the emission spectrum (Eqn.11). It is the first such attempt. Our approach requires the design of a program which can numerically evaluate Eqn.11. In what follows that program is described in brief, and displayed in full in Appendix II.

The complete program, collaboratively developed at the MP^{3}L, can be found in Appendix II. Although the following comparisons result from this program, it should be noted that Eqn.11 contains all the elements necessary to describe the rate modification of a complete spectra. An example was shown in Fig.15. The program utilizes a combination of unique asymptotics developed from fundamental results of Lam, et al,[27] and solutions for the positions and strengths of resonance positions from Eqns. 9-11 to expedite the process of fitting theory to data. A basis for these asymptotics can be found in reference 27, however the full derivation is from the unpublished results of Arnold, et al.[28] A brief description of the program is presented here.

The program requires only one initial entry of data. The physical parameters of optical size and the orientation of the surface moments must be assigned for the specific region of interest. It begins by processing the definition of several specialized functions, (e.g. spherical Bessel) as well as the relative rates of decay for both tangential and perpendicular cases (θ = 90^o or 0^o) to the normal of the surface from Eqns.9-10. The experimental parameters and spectrometer resolution are also defined. Following, is a comprehensive list of resonance positions (in

optical size, X), calculated from a FORTRAN program designed to pick solutions for a particular angular momentum, l, and polarization (TE or TM). The program proceeds to a do loop where the qualifying resonances are picked from the desired range of optical size. The asymptotics for both width and strength are also calculated within the do loop, and their result for the chosen resonances are separated into a definitive array, listing the mode number, angular momentum, TE or TM status, and most importantly, its position, width and strength. Finally, the information is convolved through a representative Lorentzian and the result plotted as a function of optical size. The user is required to enter the desired optical size for the background to be calculated, and the function is again plotted as a function of wavelength with a given background. The final result is a model spectra for the chosen orientation and optical size convolved to the experimental resolution. Unfortunately, to date, the program fails to account for all observed phenomena such as mode reabsorption[19] and the additional size dependency in background counts.[29]

Comparisons of experimental data to theory (Figs.26 and 27) were done for both Figs.21 and 22. The calculations were carried out by utilizing a complex refractive index $m = 1.47 + i\ 10^{-7}$, consistent with losses demonstrated in glycerol,[8] and have been convolved with the APMS' resolution (0.1nm). Model theoretical emission rate spectra, $\gamma(\omega)/\gamma_0$, (26 B and 27 B) for both $\theta = 90^o$ or 0^o orientations are in good agreement with the experimental emissive moment orientation of BODIPY without (26 A) and with (27 A) additional stearate respectively. The contrasting extreme orientation for either spectra are also shown in 26 C and 27 C.

Fig.26A was taken using the Acton 300i (1800 G/mm) and ST-6 detector where the calibration factor was 0.0136 nm/pixel. Calculation parameters for Fig.26B included a droplet radius of a~7.580, where the imaginary part of the refractive index was $\kappa=2.0/10^{-7}$ to account for lower order mode absorption (e.g. 4th order TE and TM strengths). The corresponding optical size, $2\pi a/\lambda$, for the spectra range (X_{min}-X_{max}), therefore corresponds to 91.06-93.02.

Fig.27A utilized the Jarrell Ash 250 (1200 G/mm) where the ST-6 detector was calibrated at 0.0379 nm/pixel. Similarly, Fig.27B was calculated for a droplet of a=7.5187, where the imaginary part of the refractive index was $\kappa=0.5/10^{-7}$. Spectral optical size range varied from 89.73-92.00.

Above selected modes in both figures are labels of the form $TE_{l\ m}$ or $TM_{l\ m}$ corresponding to the transverse electric or transverse magnetic polarization, mode number, l, and mode order, m. Noticeably, for the tangentially oriented moments (Figs.26B or Fig.27C), each TE peak is accompanied by a TM of identical order and

number within the period with the exception of the 4th order mode. In this case, the large 5th order TE peak seems to obscure the 4th order TM, indicated by the dotted lines between Fig.26 B-C and 27 B-C. However, when the TE modes are absent in $\theta = 0^o$ (Fig.26C and 27B) the 4th order TM appears with nontrivial intensity. The reality is that the optical size position between the two varies by only a few thousandths. However, in the experimental spectrum of Fig.26A, a recurring fifth resonant peak of small intensity appears in approximately the same position as the 4th order TM. Although the exact cause is not known, it is assumed that the peak is the 4th order TM since its complementary TE of the same order is within the spectra (indicated by the dashed lines of Figs.26 & 27).

For a first such attempt, the comparisons are surprisingly good, and we believe that our research is a harbinger for a new area in the surface science of liquids especially those in heterogeneous phases such as aerosol and biological spores.

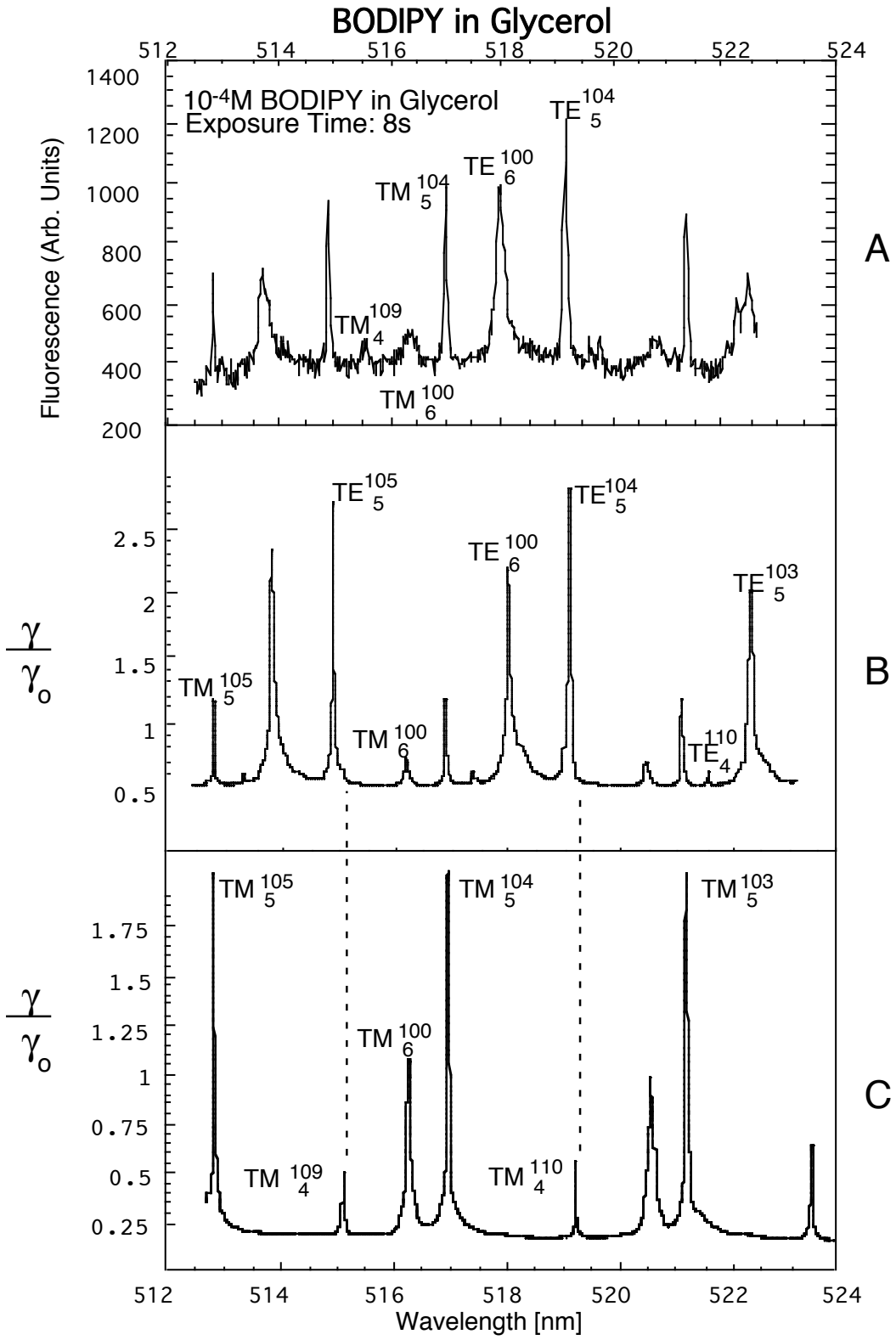

Fig.26 (A)Experimental Spectra 10^{-4}M BODIPY in Glycerol, a=7.580μm, with model Emission Rate Spectra for Surfactant Emission Moments of $\theta=90^{o}$ (B) and $\theta=0^{o}$ (C) to the surface normal

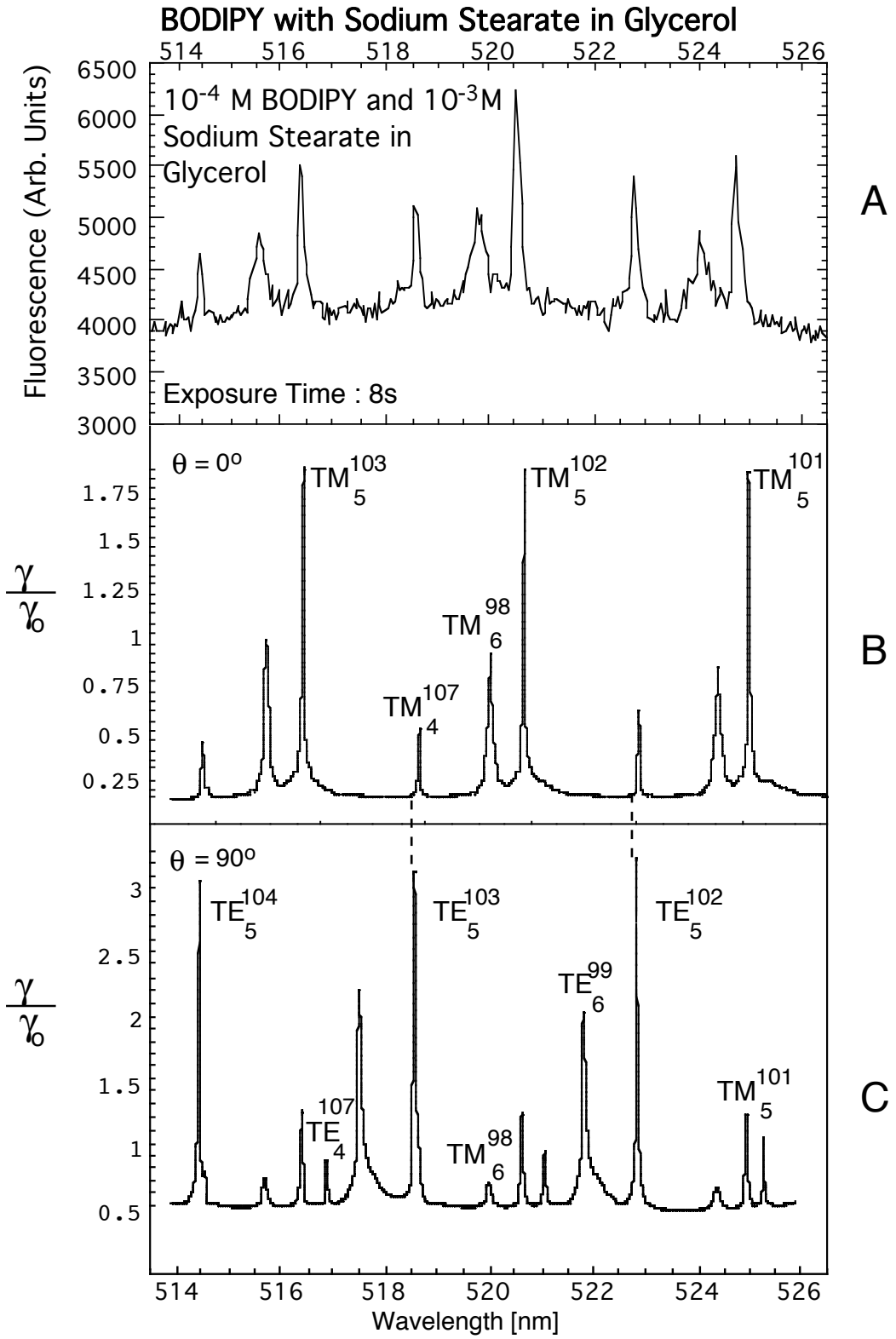

Fig.27(A)Experimental Spectra 10^{-4}M BODIPY/10^{-3}M Stearate in Glycerol, a=7.5187μm with model Emission Rates for Surfactant Emission Moments of $\theta=0^{o}$ (B) and $\theta=90^{o}$ (C) to the surface normal

VI. CONCLUSION

In summary, we have disproven the common belief that emission is a molecular property associated with the local molecular environment. Clearly it does not work, and just as the particular case can exclude the general rule, this clearly excludes the premise. Second we have found a rationale for understanding the behavior of molecular fluorescence inside a spherical particle in terms of radiation reaction theory, which we find to fit the data well. This implies that the quantum electrodynamics way of explaining similar effects must be to some extent, equivalent.[30] Additionally, we show the rate of emission to be profoundly modified by changes in the orientation of surfactant fluors.

Only limited information could be gathered from the existing levitation instrument, called the Aerosol Particle Microscope (APM). Although its previous purpose was primarily imaging, adaptations including an output to a monochromator and CCD detector converted the instrument into a spectrometer (APMS). Spectra taken through the APMS of a bicomponent system of glycerol and dilute surfactant dye, reveal a unique emission fingerprint indicative of the preferential mode coupling of the chromophore to the droplet's inherent modes. It has been shown that the addition of a third component of optically inert surfactant, compressed into a surface monolayer acts as a supportive structure to the chromophores, altering the orientation of their emissive moments toward the surface normal.[31]

Experimental spectra are compared to theoretical predictions for droplets of a chosen size, refractive index, and surfactant orientation. A computer program was developed to expedite the calculation of resonant positions from the semiclassical model, and their corresponding widths and strengths were figured through asymptotics. Convolution to the instrument's resolution was also considered so that the final output was representative of the APMS instrument's (Fig.8) capabilities for "true" comparison against experiment. The comparisons are in good agreement for two extreme orientations of emissive moments, both tangential and perpendicular, to the droplet's surface.

This newly gained theoretical understanding of our experimental systems, may have a large number scientific as well as technological applications. Not only can surfactant signatures be understood from our prepared systems, but <u>any</u> droplet's surfactant orientation should be discernible. Applications abound in fields such as aerosol science, where numerous biological aerosols exist as microencapsulates. The "fingerprinting" of aerosol particulates can be envisioned.

Here one may inquire as to the existence of microencapsulates. Other fields, such as photonic materials, can benefit by utilizing the ability to preferentially couple into specific cavity modes through orientation, lowering the overall starting threshold of devices such as lasers. Additionally, in the study of surfaces, fluorescent probing could conceivably monitor surface-layer formation as Infrared studies[32] are commonly used today. Finally, all results are expected to apply to other spontaneous processes such as spontaneous Raman scattering, opening new possibilities in the fundamental study of molecular interaction with mesoscopic structures.

Appendix I

Let us investigate the diffusion limited evaporation process for a microdroplet levitated in a gaseous environment.

An important aspect of this problem is to recognize that the solvation energy for a charge in a polar liquid renders such ions to be essentially involatile; only neutral molecules evaporate.

Consider an isolated droplet of radius a.

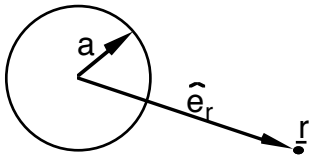

Fig A.1

Fig A.1 shows a simple schematic of an evaporating droplet, where a is the droplet radius, $\underline{r}$ is a position in the gas, and $\hat{e}_r$ is a unit vector in this direction. Since there is no source of vapor in the gas the Laplacian of the concentration will be zero in this region;

$$\nabla^2 C = 0 \tag{A1.1}$$

In spherical coordinates the complete Laplacian is

$$\nabla^2 C = \frac{1}{r}\frac{\partial^2 (r\,C)}{\partial r^2} - \frac{\hat{L}^2 C}{r^2} \tag{A1.2}$$

where $\hat{L}$ is the angular momentum operator $\hat{L} = -i\,\underline{r} \times \nabla$. Since no angular dependence for the solute vapor is expected in our spherically symmetric problem (Fig A.1), the physical problem, Eqn (A1.1) can be further simplified to

$$\frac{1}{r}\frac{\partial^2 (r\,C)}{\partial r^2} = 0 \ . \tag{A1.3}$$

The general solution to Eqn. A1.3 is

$$C = \alpha_1 + \frac{\alpha_2}{r} \quad , \tag{A1.4}$$

where α_1 and α_2 are constants resulting from indefinite integrals with respect to r. To further define C in terms of known quantities, let us consider two specific boundary conditions. At the surface, C(a) = C_s, and at an infinite distance away from the droplet, C(∞) = C_∞. Using these boundary conditions, C is found to be

$$C = (C_s - C_\infty)\frac{a}{r} + C_\infty \tag{A1.5}$$

Evaporation occurs by diffusion into the environment. The loss of mass may be described in terms of an integral of the mass flux over a sphere just outside the particle surface.

$$\frac{dm}{dt} = -\oint \underline{J} \cdot \hat{\varepsilon}_r \, dA \, , \tag{A1.6}$$

where the mass current density $\underline{J}$ is defined in terms of diffusion by Fick's Law.

$$\underline{J} = -D \nabla C \tag{A1.7}$$

The gradient of the concentration profile from Eqn. A1.5 at the radius of the particle is [- (C_s - C∞) / a] $\hat{\varepsilon}_r$ so that the integral on the right hand side of Eqn. A1.6 becomes

$$-\oint \underline{J} \cdot \hat{\varepsilon}_r \, dA = -4\pi \, a \, D(C_s - C_\infty) \, . \tag{A1.8}$$

The left hand side of Eqn. A1.6 can be written in terms of particle size and density ρ,

$$\frac{dm}{dt} = 4 \, \pi \, \rho \, a^2 \frac{da}{dt} \, . \tag{A1.9}$$

Together, Eqn.A1.8 and A1.9 allow us to arrive at the rate of change of the particle's cross section,

$$\frac{d(a^2)}{dt} = -\frac{2\,D\,(C_s - C_\infty)}{\rho} \qquad \text{(A1.10)}$$

If the radius is a at time t and a_o at t=0 then the solution to Eqn. A1.10 is

$$\left(\frac{a}{a_o}\right)^2 = 1 - \frac{2\,D\,(C_s - C_\infty)}{\rho\, a_o^2}(t - t_o) \qquad \text{(A1.11)}$$

For a levitated droplet the levitation potential, V_{dc}, is proportional to the mass so long as the charge is invariant. However, the mass is proportional to the radius cubed, and therefore the radius squared is proportional to $V_{dc}^{2/3}$. On this basis Eqn.A1.11 written in terms of levitation voltage becomes

$$\left(\frac{V_{dc}(t)}{V_{dc}(0)}\right)^{\frac{2}{3}} = 1 - \frac{2\,D\,(C_s - C_\infty)}{\rho\, a_o^2}(t - t_o) \qquad \text{(A1.12)}$$

Let us suppose for simplicity that $C_\infty = 0$ and that the concentration of solute vapor near the drop surface is dilute enough to be considered an ideal gas. On this basis C_s can be written in terms of the surface vapor pressure, P_s, and the molecular weight of the solute M_s; $C_s = P_s M_s / RT$ so that

$$\left(\frac{V_{dc}(t)}{V_{dc}(0)}\right)^{\frac{2}{3}} = 1 - \frac{2\,D\left(\frac{P_s\,M_s}{RT}\right)}{\rho\, a_o^2}(t - t_o) \qquad \text{(A1.13)}$$

References

[1]. See articles within *Optical Processes in Microcavities ,* Eds. R.K. Chang and A.J. Campillo (World Scientific Publishing, 1996).

[2]. W.B. Whitten, J.M. Ramsey, S. Arnold, and B.V. Bronk, Anal. Chem. 63 , 1027(1991).

[3]. *Shih-Ching* or "Book of Poems" 1100-1200 BC. The author noted the glow of fireflies.

[4]. Vincent Cascariolo (1603) was searching for the legendary "Philosopher's Stone" that could turn any metal into gold. Instead he found silvery white stones (barite) on Mount Paderno, near Bolonga, Italy, and found that after heating the pulvarized rocks, a faint purple-blue glow radiated. He actual reduced barium sulfate to a weakly phosphorescing barium sulfide.

[5]. R.E. Benner, P.W. Barber, J.F. Owen, R.K. Chang, Phys.Rev.Lett. 44 , 475(1980).

[6]. L.M. Folan, S.Arnold, S.D. Druger, Chem.Phys.Lett. 118 , 322 (1985).

[7]. S.D. Druger, S. Arnold, and L.M. Folan, J. Chem. Phys.87, 2649(1987).

[8]. S. Arnold and L.M. Folan, Opt. Lett. 14, 387(1989).

[9]. S. Arnold, S. Holler, and S.D. Druger, J. Chem. Phys. 104, 7741 (1996).

[10]. R.P. Feynman, *Lectures on Physics*, (Addison Wesley, Mass., 1964), Vol.1, p. 31- 4.

[11]. H. Kuhn, J. Chem. Phys. 53, 101(1970).

[12]. For a discussion of radiation reaction and other relevant physics associated with the semiclassical dipole approximation see M. Sargent, M.O. Scully and Willis E.Lamb, *Laser Physics,* (Addison-Wesley Publishing Co., London, 1974), Chap.3

[13]. Y.S. Kim, P.T. Leung, and T.F. George, Surface Sci. 195, 1(1988).

[14]. H. Chew, J.Chem.Phys. 87 , 1355 (1987)

[15]. S. Arnold and L.M. Folan, Rev. Sci. Inst. 57, 2250(1986).

[16]. S. Arnold and L.M. Folan, Microphotography on an Electrodynamically Levitated Microparticle, Proc. Soc. Photo-Opt. Instrum. Eng. 1862, 218(1993).

[17]. S. Arnold, S. Holler, J. H. Li, A. Serpengüzel, W. F. Auffermann, and S.C. Hill, Opt. Lett 20, 773-775 (1995).

[18]. M.D.Barnes, C-Y. Kung, W.B.Whitten, J.M.Ramsey, S.Arnold, and S.Holler , Phys.Rev.Lett. 76, 3931 (1996)

[19]. S. Arnold, S. Holler, N.L. Goddard, and G.Griffel, Opt.Lett. 22 ,1452 (1997).

[20]. P. Chylek, H-B. Lin, J.D. Eversole and A.J. Campillo, Opt. Lett. 16, 1723(1991).

[21]. S. Holler, N.L. Goddard and S. Arnold, J. Chem. Phys.108, 1998.

[22]. S.A. Safran. "Flexible Interfaces" *Statistical Thermodynamics of Surfaces, Interfaces, and Membranes.* Chap 6, p. 191. Addison Wesley, Mass., 1994.

[23]. J. Karolin, L B-Å Johansson, L. Strandberg, and T. Ny. Fluorescence and Absorption Spectroscopic Properties of Dipyrromethene boron Difluoride (BODIPY) Derivatives in Liquids, Lipid Membranes, and Solids. J.Am.Chem.Soc. 116, 7801-7806 (1994).

[24]. R.A. Hann. "Molecular Structure and Monolayer Properties." G. Roberts, ed. in *Languir Blodgett Films*. Chapter 2, p. 32. Plenum: New York 1990.

[25]. E.J.Davis, "Single Aerocolloidal Particle Instrumentation and Measurement", in *Surface and Colloid Science Vol.14*, Ed. by Egon Matijevic (Plemum Press, New York, 1987),pp 1-81.

[26]. C.S.Miner, N.N.Dalton. *Glycerol* . American Chemical Society Monograph Series. Reinhold: New York, 1955.

[27]. C.C.Lam, P.T.Leung, and K.Young, J.Opt.Soc.Am. B 9, 1585 (1992)

[28]. S.Arnold and S.Holler, An Asymptotic Model for Fluorescence from a Meso-optic Sphere, In preparation.

[29]. K.Miyano. University of Tokyo, Applied Physics,Unpublished Results.

[30]. P.W. Milonni. Am.J.Phys. 52, 340 (1984)

[31]. N.L. Goddard, S. Arnold, and S. Holler, Fluorescence from Monolayers on a Spherical Dielectric Microcavity (in preparation).

[32]. Paul H. Axelsen, W.David Braddock, Howard L. Brockman, Craig M. Jones, Richard A. Dluhy, Brad K. Kaufman, and Francisco J. Puga Appl.Spec. 49, 4(1995).